

RESEARCH ARTICLE

Adipose triglyceride lipase promotes prostaglandin-dependent actin remodeling by regulating substrate release from lipid droplets

Michelle S. Giedt^{1,*}, Jonathon M. Thomalla^{2,*}, Roger P. White², Matthew R. Johnson², Zon Weng Lai³, Tina L. Tootle^{1,‡,§} and Michael A. Welte^{2,‡,§}

ABSTRACT

Lipid droplets (LDs), crucial regulators of lipid metabolism, accumulate during oocyte development. However, their roles in fertility remain largely unknown. During *Drosophila* oogenesis, LD accumulation coincides with the actin remodeling necessary for follicle development. Loss of the LD-associated Adipose Triglyceride Lipase (ATGL) disrupts both actin bundle formation and cortical actin integrity, an unusual phenotype also seen when the prostaglandin (PG) synthase Pxt is missing. Dominant genetic interactions and PG treatment of follicles indicate that ATGL acts upstream of Pxt to regulate actin remodeling. Our data suggest that ATGL releases arachidonic acid (AA) from LDs to serve as the substrate for PG synthesis. Lipidomic analysis detects AA-containing triglycerides in ovaries, and these are increased when ATGL is lost. High levels of exogenous AA block follicle development; this is enhanced by impairing LD formation and suppressed by reducing ATGL. Together, these data support the model that AA stored in LD triglycerides is released by ATGL to drive the production of PGs, which promote the actin remodeling necessary for follicle development. We speculate that this pathway is conserved across organisms to regulate oocyte development and promote fertility.

KEY WORDS: Actin cytoskeleton, Lipid droplets, Prostaglandin signaling, *Drosophila*, Oogenesis

INTRODUCTION

Rates of infertility are increasing (Sun et al., 2019). Fertility requires the production of high-quality oocytes. Among key factors ensuring oocyte quality are the amount and types of lipids present during oogenesis (Dunning et al., 2014; Brusentsev et al., 2019). In mammalian follicles, fatty acids (FAs) likely contribute a crucial source of energy as inhibitors of FA oxidation impair oocyte maturation (Dunning et al., 2010, 2011). Lipid signaling molecules – from steroid hormones to eicosanoids – control diverse aspects

of oocyte development and fertility (Prates et al., 2014). Prostaglandins (PGs), a class of eicosanoids, regulate oocyte development, ovulation, fertilization, implantation, maintenance of pregnancy, and childbirth (Tootle, 2013; Sugimoto et al., 2015). Thus, control of lipid metabolism is central for oocyte development and fertility, yet few underlying mechanisms are known.

Key regulatory steps in lipid metabolism are mediated by lipid droplets (LDs), cellular organelles that store neutral lipids (Walther and Farese, 2012). LDs stockpile excess amounts of cholesterol and related sterols as sterol esters, and safely sequester toxic FAs in the form of triglycerides. Such FAs are released by LD-bound lipases to be shuttled to mitochondria for oxidative breakdown, used to generate membrane precursors, or turned into signaling molecules (Welte, 2015). Given that both triglycerides and LDs are abundant in oocytes, LDs may perform similar roles during oogenesis. Indeed, LD accumulation, composition and localization are dynamic during oocyte maturation across organisms (Ami et al., 2011; Dunning et al., 2014; Brusentsev et al., 2019), and, in the context of obesity, changes in oocyte LDs are associated with infertility (Jungheim et al., 2010; Cardozo et al., 2011; Marei et al., 2020). However, the functions of LDs in oogenesis remain largely undefined.

A promising model for uncovering the roles of LDs is *Drosophila* oogenesis. Adult female flies have two ovaries, each comprising ~15 ovarioles or chains of sequentially maturing follicles, also called egg chambers. Each follicle is made up of ~1000 epithelial follicle cells and 16 germline cells (15 nurse cells and one oocyte). Follicles develop over the course of ~10 days through 14 stages. In mid-oogenesis, LDs undergo dramatic changes (Fig. 1A–D) (Buszczak et al., 2002). Prior to Stage 8 (S8), only a few scattered LDs are found throughout the follicle. In S9, LD biogenesis is massively upregulated in the nurse cells, so that by S10B the nurse cell cytoplasm is full of uniformly sized LDs (~0.5 µm in diameter) (Buszczak et al., 2002; Teixeira et al., 2003). Thus, in just a few hours, nurse cells form tens of thousands of LDs. During S11, the LDs are transferred into the oocyte in a process termed nurse cell dumping, in which cytoplasmic contents of the nurse cells are squeezed into the oocyte through intercellular bridges called ring canals. These LDs provide the future embryo with stores of energy and specific proteins needed for development (Welte, 2015); indeed, embryos with reduced LDs have decreased hatching probability (Teixeira et al., 2003; Parra-Peralbo and Culi, 2011). Whether these LDs only provision the embryo or if they play roles in follicle development remains unclear.

One potential role of LDs during oogenesis may be to regulate lipid signaling. One class of lipid signaling molecules, PGs, plays crucial roles during mid-oogenesis. PGs are derived from arachidonic acid (AA), a poly-unsaturated FA, which is converted first into PGH₂ and then immediately processed into one of several types of bioactive PGs (Tootle, 2013). These enzymatic steps are mediated by cyclooxygenase (COX) enzymes and specific PG

¹Anatomy and Cell Biology, University of Iowa Carver College of Medicine, Iowa City, IA 52242, USA. ²Department of Biology, University of Rochester, Rochester, NY 14627, USA. ³Harvard T.H. Chan Advanced Multi-omics Platform, Harvard T.H. Chan School of Public Health, Boston, MA 02115, USA.

*These authors contributed equally to this work

‡These authors contributed equally to this work

§Authors for correspondence (tina-tootle@uiowa.edu; michael.welte@rochester.edu)

ORCID M.S.G., 0000-0002-5720-8326; J.M.T., 0000-0003-3968-4764; T.L.T., 0000-0002-1515-9538; M.A.W., 0000-0001-5741-4720

This is an Open Access article distributed under the terms of the Creative Commons Attribution License (<https://creativecommons.org/licenses/by/4.0>), which permits unrestricted use, distribution and reproduction in any medium provided that the original work is properly attributed.

Handling Editor: Thomas Lecuit

Received 7 December 2022; Accepted 3 May 2023

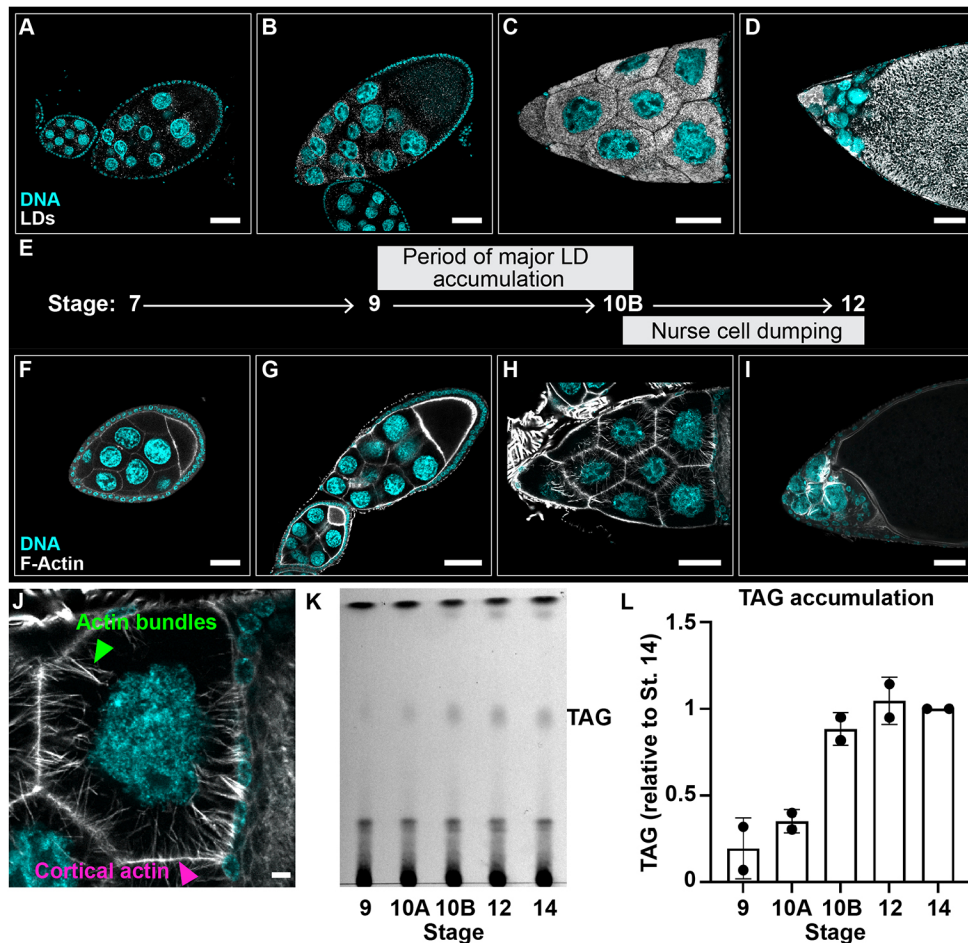


Fig. 1. LD accumulation and actin cytoskeletal remodeling occur during mid-oogenesis. (A-I) Single confocal slices of wild-type (Oregon R) follicles of the indicated stages (E) stained for LDs (Nile Red, A-D) or F-Actin (phalloidin, F-I) in white, and DNA (Hoechst) in cyan. Scale bars: 50 μ m. (E) Schematic depicting the progression of LD accumulation and actin remodeling during oogenesis. All of the images and the schematic in A-I are positioned on top of a black background. (J) Confocal slice of an S10B nurse cell stained for F-Actin (phalloidin) in white and DNA (Hoechst) in cyan; arrowheads indicate actin bundles (green) and cortical actin (magenta). Scale bar: 10 μ m. (K) Thin layer chromatograph of whole-lipid extracts from late-stage follicles. (L) Quantification of TAG levels in K plotted relative to S14; error bars represent s.d. LDs begin to accumulate during S9 (B), are present in large numbers and evenly distributed throughout the nurse cell cytoplasm in S10B (C), are dumped into the oocyte during S11 and are highly abundant in the ooplasm by S12 (D). This temporal accumulation is reflected by increases in triglycerides and sterol esters (K,L), neutral lipids stored in LDs. Massive remodeling of the nurse cell actin cytoskeleton begins when LDs are highly abundant (E-H). The cortical actin thickens and actin bundles extend from the membrane to the nucleus during S10B (H). During S11, actin bundles hold the nurse cell nuclei in place while the cortical actin contracts, squeezing the cytoplasm into the oocyte (nurse cell dumping), causing oocyte expansion (I).

synthases, respectively. *Drosophila* has a single COX-like enzyme called Pxt, and its absence results in severe defects in the actin remodeling necessary for late-stage follicle morphogenesis; this ultimately causes female sterility (Tootle and Spradling, 2008; Spracklen and Tootle, 2015). During S10B, the nurse cell actin cytoskeleton is remodeled: parallel actin bundles extend from the plasma membrane to the nuclei to form a cage, and the cortical actin substantially thickens (Fig. 1F-J). Both of these actin structures are required during S11 for nurse cell dumping; the cortical actin provides contractile force and the actin bundles prevent nuclei from being pushed into the ring canals and plugging them (Wheatley et al., 1995; Guild et al., 1997; Huelsmann et al., 2013). Loss of Pxt results in severe disruption in actin bundle formation, breakdown of cortical actin, and failure of nurse cell contraction (Tootle and Spradling, 2008; Spracklen and Tootle, 2015). Genetic studies have revealed that PG signaling regulates the activity of actin-binding proteins, including Fascin (Singed) and Enabled, to drive the actin remodeling necessary for follicle morphogenesis (Groen et al., 2012; Spracklen et al., 2014, 2019). However, how PG production is temporally and spatially regulated during *Drosophila* oogenesis remains unknown, but in many cells the release of AA from cellular lipids is the rate-limiting step (Funk, 2001; Tootle, 2013). Those precursor lipids are primarily thought to be phospholipids in cellular membranes, but in mammalian immune cells neutral lipids are a source of AA for PG synthesis (Dichlberger et al., 2014; Schlager

et al., 2015). This raises the question of whether LD accumulation during *Drosophila* mid-oogenesis supports PG synthesis.

We sought to determine whether LDs contribute to *Drosophila* follicle development. Loss of the LD-associated Adipose Triglyceride Lipase (ATGL; Brummer) results in *pxt*-like actin remodeling defects during S10B. The similar phenotypes led us to ask whether ATGL and Pxt function in the same pathway during *Drosophila* oogenesis. Dominant genetic interaction and rescue experiments indicate that ATGL acts upstream of PG synthesis to drive actin remodeling. Further, lipidomic and exogenous AA experiments lead to the model that AA is stored in LDs, and ATGL is required to release AA from LDs to provide the substrate for PG production. Ultimately, these PGs control actin remodeling and thereby follicle development. These studies uncover new roles for LDs in regulating oogenesis, to sequester a developmentally important molecule, AA, and to control its release to drive specific processes.

RESULTS

ATGL is required for actin remodeling in nurse cells

During *Drosophila* oogenesis, LDs undergo dramatic changes in just a few hours (Fig. 1A-E). LDs start to accumulate at S9, fill the nurse cells by S10B, and are transferred to the oocyte by S12. In most tissues, the main neutral lipids stored in LDs are triglycerides and/or sterol esters (Walther and Farese, 2012). Using thin-layer chromatography, we found that developing follicles accumulate

both classes of neutral lipids and triglyceride accumulation measured biochemically mirrors LD accumulation detected by microscopy (Fig. 1K,L).

Previous *in situ* hybridization experiments found that *ATGL* is highly expressed in nurse cells during mid-oogenesis, just as LDs accumulate (Jambor et al., 2015). As *ATGL* catalyzes the conversion of triacylglycerol to diacylglycerol and free FA (Grönke et al., 2005), this pattern raises the possibility that LD triglycerides are broken down during these stages. Using an endogenously tagged *ATGL-GFP* allele (Zhao et al., 2022), we confirmed that *ATGL* is expressed in S10B follicles and colocalizes with LDs (Fig. 2A-A''). We also separated LDs from other cellular components by *in vivo* centrifugation: when living *Drosophila* follicles are centrifuged, their contents separate by density within each nurse cell/oocyte, with LDs accumulating on the side that faced up during centrifugation (Cermelli et al., 2006; Li et al., 2012). Staining of fixed centrifuged S10B follicles revealed that *ATGL-GFP* is enriched in the LD layer (Fig. 2B-B'').

As LD accumulation coincides with PG-dependent actin remodeling during S10B (Fig. 1E), we investigated whether *ATGL* has a role in these events. We found that females lacking *ATGL* display two types of actin defects (Fig. 3). First, actin bundles are aberrant. Some nurse cell membranes lack bundles, and the bundles that form are short, abnormally distributed, and/or fail to project toward the nuclei (Fig. 3B,B', green arrowheads). Second, cortical actin is broken down, leading to the appearance of multinucleate nurse cells (Fig. 3B,B', magenta arrowheads). To quantify these defects, we acquired confocal stacks of phalloidin-stained S10B follicles and separately scored actin bundles and cortical actin as having no (normal), mild, moderate or severe defects. We then summed these scores to give an actin defect index (ADI) to classify each follicle into three categories: normal, mild

defects or severe defects (see Materials and Methods and Fig. S1 for details). Loss of *ATGL* resulted in actin bundle defects in ~83% of the follicles (Fig. 3D) and cortical actin breakdown in ~50% (Fig. 3E), with about a quarter of follicles exhibiting a severe ADI (Fig. 3F).

This combination of actin defects is rarely seen, as most actin regulators impact either actin bundle formation or cortical actin, but not both (Wheatley et al., 1995; Buszczak and Cooley, 2000). However, the same combination of phenotypes was observed when PG signaling is lost: lack of the COX-like enzyme *Pxt* caused collapsed, stunted or absent actin bundles, and cortical actin breakdown with a failure of nurse cell contraction (Fig. 3C,C') (Tootle and Spradling, 2008; Spracklen and Tootle, 2015). Loss of *Pxt* resulted in actin bundle defects in ~87% of the follicles and cortical actin breakdown in ~76% (Fig. 3D,E), corresponding to a severe ADI for over 63% of the follicles (Fig. 3F). Thus, loss of *Pxt* and *ATGL* results in the same unusual combination of phenotypes.

***Pxt* functions in a linear pathway with *ATGL* to regulate actin remodeling**

The similar actin phenotypes in *pxt* (*Pxt*; FBgn0261987) and *ATGL* mutants suggest they may act in the same pathway to regulate actin remodeling. To test this hypothesis, we used a dominant genetic interaction assay, taking advantage of the fact that heterozygosity for the individual mutations (*pxt*^{-/+} or *ATGL*^{-/+}) has limited effects on actin remodeling (Fig. 4A,B). We can therefore use heterozygosity for *pxt* (*pxt*^{-/+}) as a sensitized background to investigate whether reducing *ATGL* levels causes actin remodeling defects (Fig. S2). If *ATGL* and *Pxt* function in the same pathway, then double heterozygotes for *ATGL* and *pxt* (*ATGL/pxt*) will exhibit severe actin defects. Conversely, if they function in separate

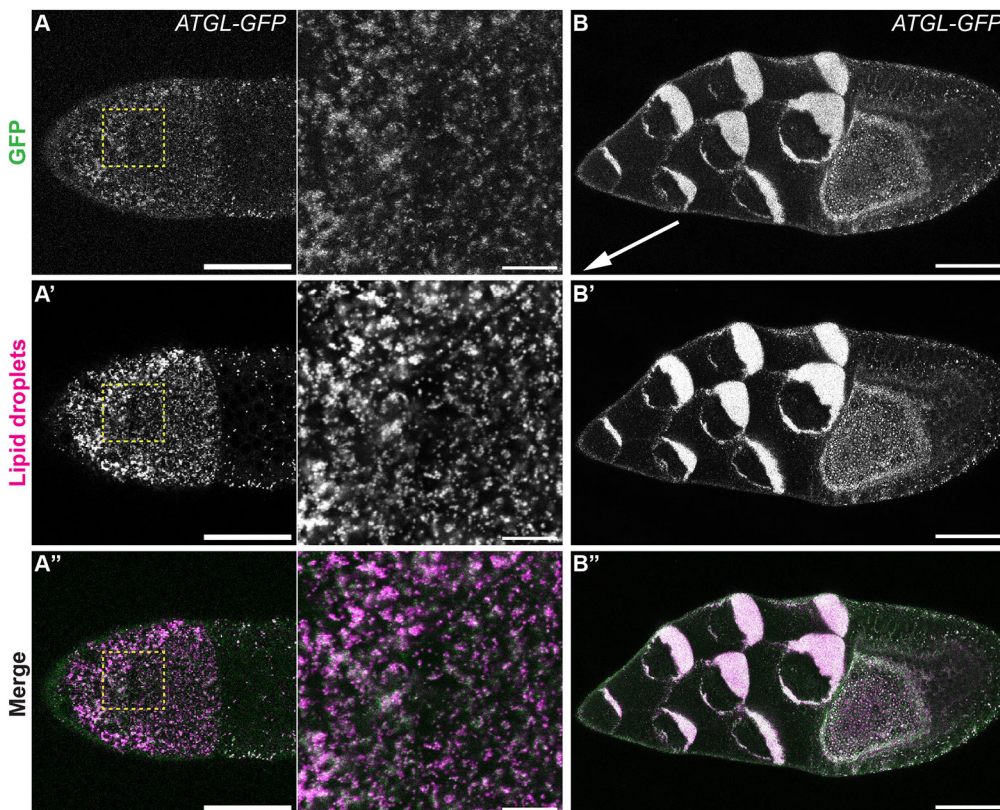


Fig. 2. *ATGL* is expressed in S10B nurse cells and localizes to lipid droplets. (A-A'') Confocal slice of *ATGL-GFP* (green in merge) expressing S10B follicle stained for LDs (LipidSpot, magenta in merge); boxed regions are shown at higher magnification on the right. Note that a focal plane near the nurse cell surface was chosen as LD density there is lower than in the center, making colocalization easier to judge. (B-B'') Confocal slice of S10B centrifuged follicle expressing *ATGL-GFP* (green in merge) stained for LDs (LipidSpot, magenta in merge). Orientation during centrifugation is indicated by the arrow (which points towards the center of rotation). *ATGL* localizes to lipid droplets in S10B follicles (A-B''). Scale bars: 50 μ m (main panels); 10 μ m (right-hand panels in A-A'').

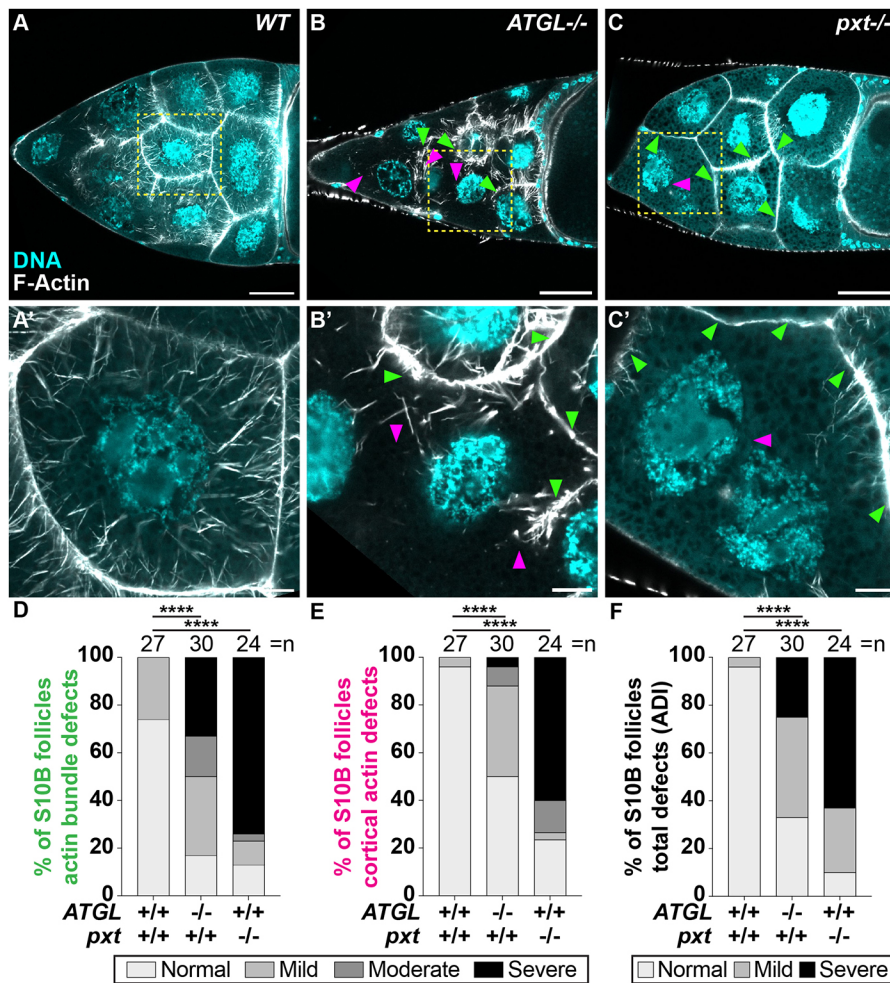


Fig. 3. ATGL regulates actin bundling and cortical actin integrity in S10B follicles.

(A-C') Confocal slices of S10B follicles stained for F-Actin (phalloidin) in white, and DNA (DAPI) in cyan; yellow boxed regions are shown at higher magnification in A'-C'. Arrowheads indicate examples of actin bundling (green) and cortical actin (magenta) defects. Scale bars: 50 μ m (A-C); 10 μ m (A'-C'). (A,A') WT, wild type (*yw*). (B,B') *ATGL*^{-/-} (*bmm*¹/*bmm*¹). (C,C') *pxt*^{-/-} (*pxt*^{#01000}/*pxt*^{#01000}). C' was taken in a different focal plane to improve visualization of the defects. (D-F) Quantification of actin phenotypes from the following genotypes: WT, *yw*; *ATGL*^{-/-}, *bmm*¹/*bmm*¹; *pxt*^{-/-}, *pxt*^{#01000}/*pxt*^{#01000}, *pxt*^{EY03052}/*pxt*^{EY03052}. Actin bundles (D) and cortical actin (E) phenotypes were scored as normal, or mild, moderate or severe defects. Scores in D,E were summed and the total binned into three actin defect index (ADI) categories: normal, mild and severe. For a detailed description of actin scoring, please see Materials and Methods and Fig. S1. *****P*<0.0001, Pearson's Chi-squared test. Error bars represent s.d. In wild-type late-S10B follicles, actin bundles extend from the nurse cell periphery to the nucleus, and the cortical actin is thickened (A,A'). Actin bundles fail to form or form improperly, and cortical actin is disrupted upon loss of ATGL (B,B',D-F) or Pxt (C,C',D-F).

pathways, actin defects in the double heterozygotes will remain low or be additive with respect to the defects in the single heterozygotes. Strikingly, the double heterozygotes had severe actin defects (Fig. 4C-F). Single heterozygotes (*ATGL*^{-/+} or *pxt*^{-/+}) exhibited mild defects in actin bundles, with ~7% being severe, whereas double heterozygotes (*pxt/ATGL*) exhibited ~22% with severe bundle defects (Fig. 4D). Cortical actin defects were rare in the single heterozygotes, with over 87% being normal; conversely, only 52% of the double heterozygotes were normal (Fig. 4E). Using our ADI quantification, most heterozygous follicles were rated as normal (84% for *ATGL*^{-/+} and 87% for *pxt*^{-/+}), whereas only 46% of the double heterozygotes exhibited normal actin remodeling; the frequency of severe cases increased from 3% in the single heterozygotes to 22% in the double heterozygotes (Fig. 4F). This synergistic increase in actin defects indicates that ATGL and Pxt regulate actin remodeling during S10B via a shared pathway.

ATGL acts upstream of Pxt

Our genetic analysis indicates that ATGL and Pxt act in the same pathway to regulate actin remodeling but does not address whether ATGL acts upstream of Pxt or vice versa. For example, PGs produced by Pxt might control ATGL levels or promote binding of actin regulators to ATGL and thus to LDs; indeed, actin-binding proteins localize to LDs in various cell types (Pfisterer et al., 2017; Bersuker et al., 2018; Tan et al., 2021). Alternatively, ATGL might control Pxt expression or the availability of Pxt's substrate to ultimately control PG synthesis levels. Unfortunately, there is no

available means of overexpressing ATGL in the germline to test whether it suppresses the actin defects in *pxt* mutants nor can we measure PG production in S10B follicles. PGs are produced at picogram levels and have extremely short half-lives (~30 s); it is impossible to isolate enough tissue to analyze PGs by either enzyme-linked immunosorbent assay or high-performance liquid chromatography-mass spectrometry.

To circumvent these limitations, we took advantage of our *in vitro* egg maturation (IVEM) assay, in which isolated S10B follicles mature *in vitro* in a simple culture medium (Spracklen and Tootle, 2013). Maturation requires PG-dependent actin remodeling as both loss of Pxt or treatment with COX inhibitors, such as aspirin, impairs *in vitro* follicle development (Tootle and Spradling, 2008). In both cases, the block in development can be suppressed by exogenous PGF_{2 α} (Tootle and Spradling, 2008); a stabilized PGF_{2 α} analog, Fluprostenol (Flu), is used. This rescue is not complete, which could be due to PGF_{2 α} not being provided at the correct level or time, or it could indicate that other PGs also contribute. In either case, if ATGL acts upstream of Pxt, PGF_{2 α} should similarly suppress defects resulting from the loss of ATGL. If, in contrast, Pxt acts upstream of ATGL, PGF_{2 α} should not modulate the *ATGL* mutant phenotype.

Using the IVEM assay, we first verified the genetic interaction between Pxt and ATGL. As expected, the majority of S10B follicles from single heterozygotes of *pxt* and *ATGL* developed *in vitro*, whereas over half of the follicles from double heterozygotes failed to develop (Fig. 5A). These data recapitulate what we observed

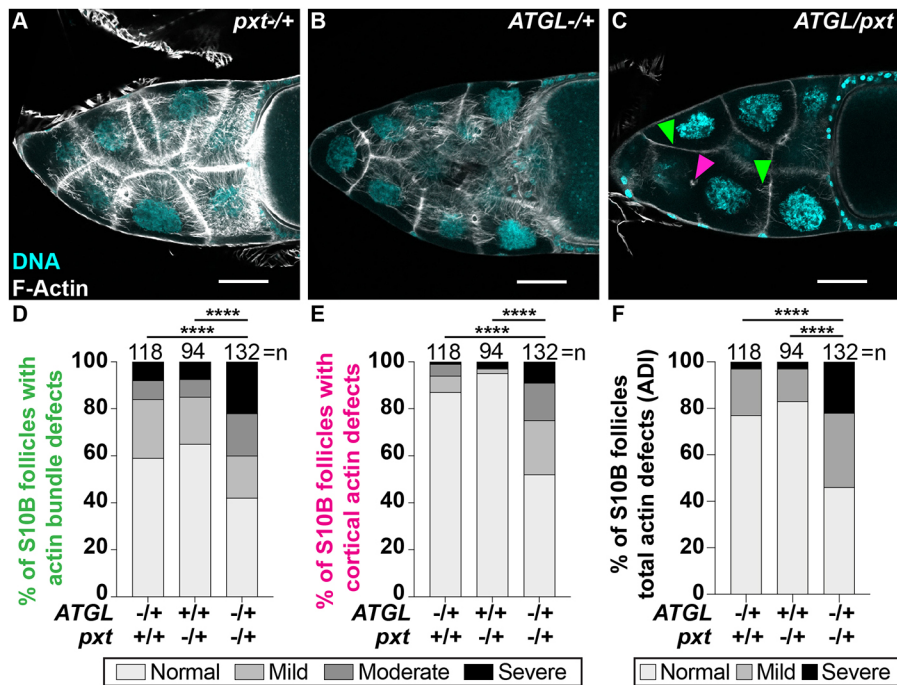


Fig. 4. ATGL acts in a linear pathway with Pxt to regulate actin remodeling. (A-C) Maximum projections of three confocal slices of S10B follicles stained for F-Actin (phalloidin) in white, and DNA (DAPI) in cyan. Arrowheads indicate examples of actin bundling (green) and cortical actin (magenta) defects. Images were brightened by 30% to increase clarity. Scale bars: 50 μ m. (A) *pxt*^{-/-} (*pxt*^{EY01000/+}). (B) *ATGL*^{-/-} (*bmm*^{1/+}). (C) *ATGL/pxt* (*bmm*^{1/pxt}^{EY01000}). (D-F) Quantification of actin bundling (D), cortical actin (E) and ADI (F) as described for Fig. 3D-F from the following genotypes: *pxt*^{-/-}, *pxt*^{EY01000/+} and *pxt*^{EY03052/+}; *ATGL*^{-/-}, *bmm*^{1/+}; *ATGL/pxt*, *bmm*^{1/pxt}^{EY01000} and *bmm*^{1/pxt}^{EY03052}. *****P*<0.0001, Pearson's Chi-squared test. Error bars represent s.d. Actin bundles and cortical actin integrity are largely normal in *pxt*^{-/-} and *ATGL*^{-/-} follicles (A,B,D-F). In contrast, in *ATGL/pxt* follicles actin bundles are absent, sparse and stunted, and there are instances of cortical actin breakdown (C-F).

when we quantified actin defects in the double heterozygotes (Fig. 4D-F). We then tested the role of PGF_{2 α} downstream of ATGL. When treated with 1.5 mM aspirin, only ~40% of wild-type S10B follicles developed, and this defect was partially suppressed by addition of PGF_{2 α} (~59% developing; Fig. 5B). Of the *ATGL* mutant follicles, only ~40% developed, but addition of PGF_{2 α} resulted in significant improvements (~63% developing; Fig. 5B). Thus, the extent of the rescue was very similar for the two cases, suggesting that Pxt and PGF_{2 α} act downstream of ATGL.

AA is present in ovary triglycerides

How does ATGL function upstream of PGs? ATGL might regulate the expression of Pxt, but that is not the case, as loss of ATGL does not alter Pxt levels (Fig. S3). Studies in mammalian cells suggest an alternative possibility. There, ATGL (PNPLA2) releases AA from triglycerides stored in LDs to serve as the substrate for COX enzymes (Dichlberger et al., 2014). If ATGL similarly generates the substrate for Pxt, *Drosophila* follicles should have AA-containing triglycerides.

As flies are thought to lack the desaturases necessary to synthesize polyunsaturated fatty acids such as AA (Shen et al., 2010), AA in triglycerides is derived from the diet. We, therefore, fed flies food supplemented with fluorescently labeled AA for ~12 h to assess AA localization in S10B follicles. AA became concentrated in puncta throughout the nurse cell cytoplasm; these structures are LDs, based on co-staining with a LD-specific dye and enrichment of AA in the LD layer of centrifuged follicles (Fig. S4). Thus, AA present in the diet can reach the ovary where it accumulates in LDs.

Next, we raised wild-type and *ATGL* mutant flies on regular food, extracted lipids from their ovaries, and analyzed those lipids by liquid chromatography with tandem mass spectrometry (LC-MS/MS). Among the 98 different triglyceride species identified (Table S1), two contained a 20-carbon FA with four double bonds (20:4), presumably AA. AA was relatively rare, making up in the order of 0.06-0.07% of all FAs detected in triglycerides (Fig. 6A),

with four other FA species accounting for the bulk (~85%) of FAs: the mono-unsaturated palmitoleic (16:1) and oleic (18:1) acids, and the saturated myristic (14:0) and palmitic (16:0) acids. We did not detect AA in the phospholipids identified in our analysis (Table S1).

The content of phospholipids (Fig. 6C) and total triglycerides (Fig. 6D) were not significantly different between wild-type and *ATGL* mutant ovaries. The overall FA profile in triglycerides was also similar between the two genotypes (Fig. 6A,B). In addition, there was no significant difference in total triglycerides in S14 oocytes, as detected by thin layer chromatography (Fig. 6E,F), even though we could confirm the previously described reduced triglyceride loading in our positive control, *PLIN2* (*Lsd-2*) mutants (Teixeira et al., 2003). Thus, ATGL-mediated lipolysis during oogenesis does not appear to lead to bulk turnover of LDs and may be restricted to supporting lipid signaling.

Supporting this possibility, wild-type and *ATGL* mutant ovaries exhibited differences in the AA-containing triglycerides, both of which were elevated in the absence of ATGL (Fig. 6G,H). This trend persisted even when measurements were normalized to all lipids in the sample (Fig. S5). These observations are consistent with the possibility that in the *ATGL* mutants less AA is released from triglycerides, resulting in a reduced pool of free AA available for signaling.

ATGL promotes AA release from LDs

Our lipidomic and imaging data suggest that AA is stored as triglycerides in LDs and its release from LDs is diminished or blocked in *ATGL* mutants. In an attempt to circumvent this block and directly provide free substrate for Pxt, we incubated isolated follicles with media containing fluorescently labeled AA. Monitoring AA localization by live imaging and *in vivo* centrifugation, we found that such exogenous AA predominantly accumulates in nurse cell LDs (Fig. 7A-B''). A similar pattern has also been observed in other systems, where exogenously applied AA is first routed to LDs (Weller and Dvorak, 1994; Bozza et al., 2009, 2011). One reason this may occur is that free AA is toxic at

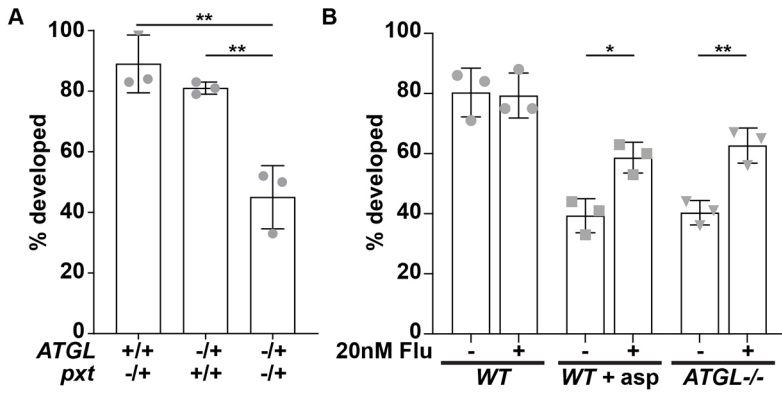


Fig. 5. ATGL functions upstream of PGF_{2α}. (A,B) Percentage of S10B follicles developing in the IVEM assay. In A, data are normalized to wild-type (*yw*) development for the following genotypes: *ATGL*^{-/-} (*bmm*^{1/+}), *pxt*^{-/-} (*pxt*^{f01000/+}) and *ATGL/pxt* (*bmm*^{1/pxt}^{f01000}). In B, wild-type (*yw*) and *ATGL*^{-/-} (*bmm*^{1/bmm}) follicles were treated with control (ethanol), 1.5 mM aspirin in ethanol, and/or 20 nM PGF_{2α} analog (fluprostenol, Flu). **P*<0.05, ***P*<0.005 (unpaired, two-tailed *t*-test). Error bars represent s.d. *ATGL* and *Pxt* interact genetically, as *ATGL/pxt* follicle development is reduced by ~50% compared with the *ATGL*^{-/-} and *pxt*^{-/-} controls (A). Aspirin treatment or loss of *ATGL* reduces the percentage of follicles developing in control media. In both cases, this is suppressed by exogenously supplying a PGF_{2α} analog (B).

near physiological levels in many cells (Pompeia et al., 2003), and, thus, sequestering AA into LDs prevents free AA from reaching toxic levels.

If exogenous AA is similarly toxic to follicles, it will preclude its use to rescue PG production. We therefore assessed the dose-dependent effects of AA on wild-type S10B follicle development with a modified IVEM assay. One of the IVEM medium's key components is fetal bovine serum (FBS), which supplies growth factors and numerous nutrients, including unknown amounts of FAs

such as AA. Thus, we reduced the amount of FBS from 10% to 2.5%, which allows most follicles to mature, and then assessed the effects of AA. At ~60 μM AA, a slightly higher percentage of follicles developed than in control medium, but that fraction dropped steadily as AA concentrations were raised (Fig. 7C). Notably, oleic acid (OA) did not impair follicle development at any concentration (Fig. 7C). Thus, it is specifically free AA that is dangerous to the follicles, which provides a rationale for why free AA is rapidly sequestered into LDs.

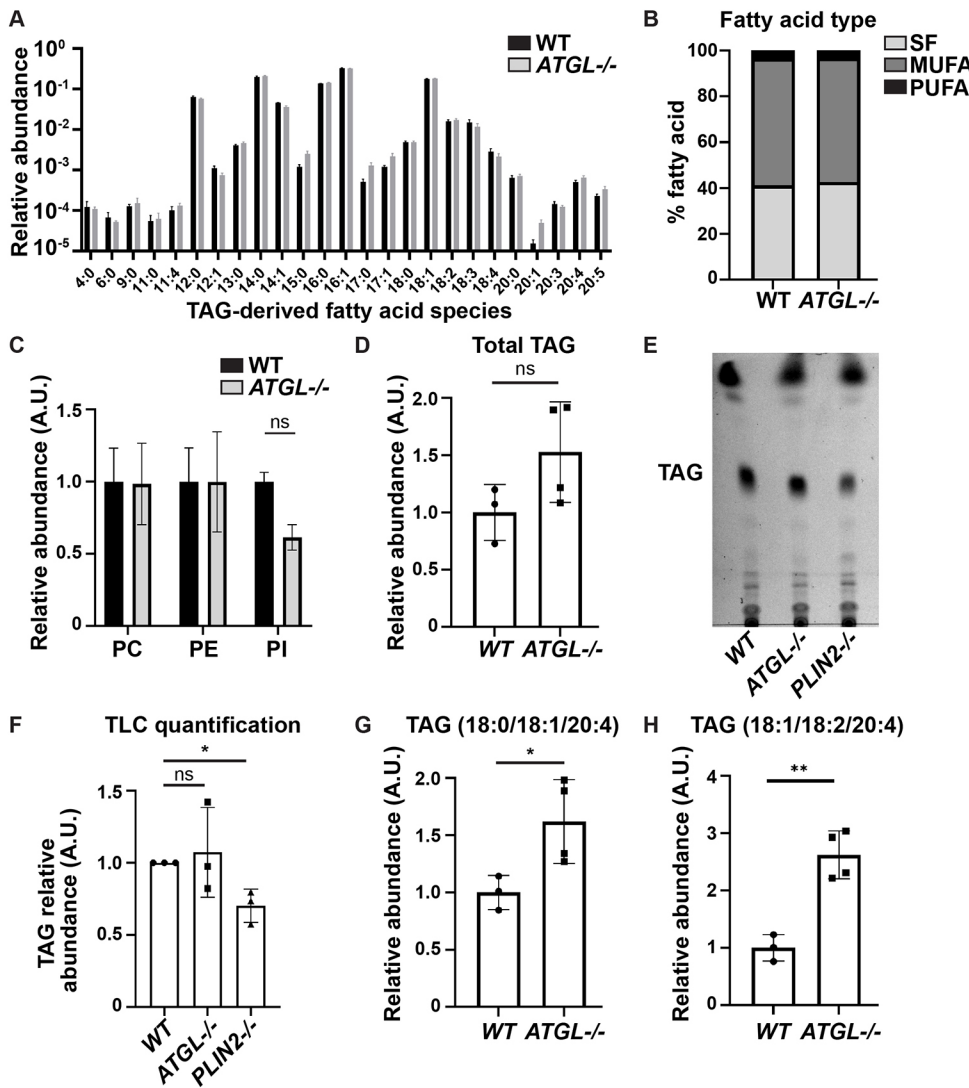


Fig. 6. Ovary triglycerides contain arachidonic acid. (A-F) Lipids were extracted from wild-type (WT; Oregon R) and *ATGL*^{-/-} (*bmm*^{1/bmm}) ovaries and analyzed by mass spectrometry. Error bars represent s.d. (A) Abundance of individual FAs in triglycerides (TAGs) expressed as fraction of all such FAs; Šídák's multiple comparisons test. (B) Total amount of saturated (SF), monounsaturated (MUFA) or polyunsaturated (PUFA) FAs relative to all FAs in TAGs; Tukey's multiple comparisons test. (C) Levels of the three phospholipid classes phosphatidylcholine (PC), phosphatidylethanolamine (PE) and phosphatidylinositol (PI); Šídák's multiple comparisons test. (D) Overall TAG levels. ns=*P*=0.1239 (two-tailed, unpaired *t*-test). (E) Thin layer chromatograph of whole-lipid extracts from S14 follicles of the indicated genotypes. (F) Quantification of TAG in E normalized to the wild type on each plate, **P*=0.0111 (two-tailed, paired *t*-test). (G,H) Quantification of two TAG species containing AA. **P*=0.0419, ***P*=0.0019 (two-tailed, unpaired *t*-tests). A.U., arbitrary units. Wild-type and *ATGL* mutant ovaries exhibit a similar abundance of FAs in TAGs (A,B), phospholipids (C), and total TAGs (D) by lipidomic analysis (no significant differences detected). Similarly, thin layer chromatographic analysis of S14 follicles reveals no differences in TAGs (E,F). Two AA-containing TAG species are present in wild-type ovaries, and their levels are elevated in the absence of *ATGL* (G,H).

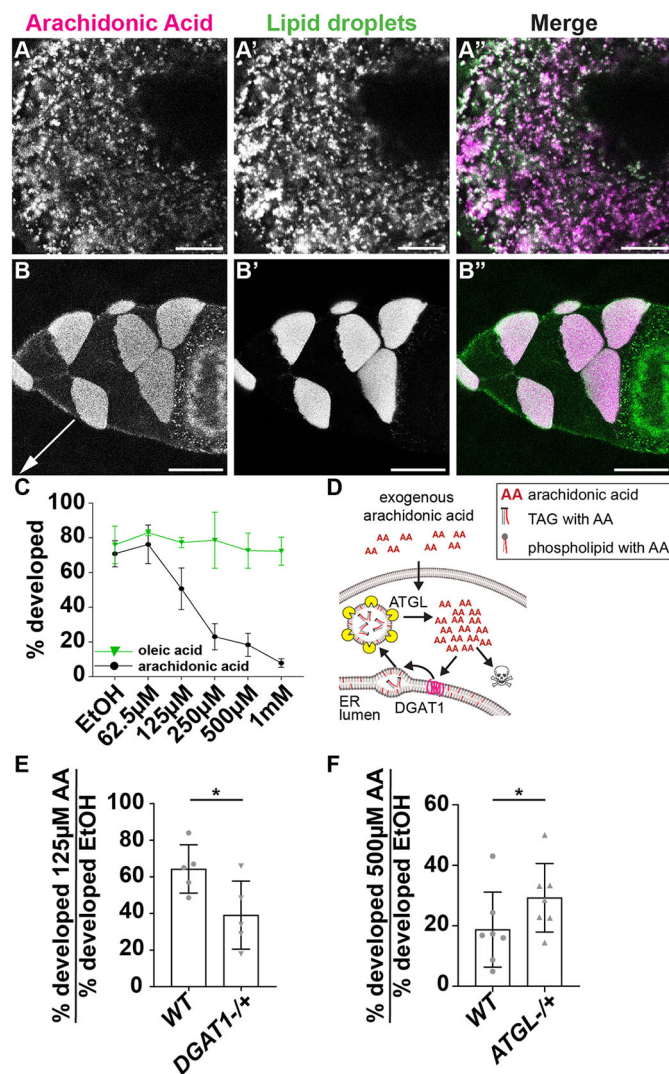


Fig. 7. ATGL regulates the release of arachidonic acid from lipid droplets. (A-B') Confocal slices of live (A-A') or centrifuged (B-B') wild-type (Oregon R, orientation during centrifugation indicated by arrow) follicles treated with NBD AA (green in merge) and LipidSpot (magenta in merge). Note that in A-A' a focal plane near the nurse cell surface was chosen as LD density there is lower than in the center, making colocalization easier to judge. Scale bars: 10 μm (A-A'); 50 μm (B-B'). (C) Dose curve of the percentage of wild-type (*yw*) S10B follicles developing in the modified IVEM assay with increasing concentrations of AA (black circles and line) or oleic acid (green triangles and line). EtOH, ethanol. Error bars represent s.d. (D) Schematic depicting how LDs may buffer AA toxicity. Exogenous AA is rapidly sequestered into LDs by DGAT1, and ATGL can release AA from LD triglycerides. Too much free AA is toxic. (E,F) Percentage of S10B follicles developing in the modified IVEM assay for the indicated genotypes and conditions. Error bars represent s.d., **P*<0.05 (two-tailed, paired *t*-test). In E, wild-type (WT, *yw*) and *DGAT1*^{-/-} (*mdy^{OX25j}/+*) follicles were treated with 125 μM AA (intermediate dose). In F, wild-type (WT, *yw*) and *ATGL*^{-/-} (*bmm¹/+*) follicles were treated with 500 μM AA (high dose). AA is present in LDs, but AA uptake varies between LDs (A-B'). High levels of AA, but not oleic acid, suppress S10B follicle development (C). Reducing the level of DGAT1, which is expected to decrease AA incorporation into LDs, enhances the ability of an intermediate dose of AA to block *in vitro* development (E). Conversely, reducing ATGL suppresses the ability of a high dose of AA to block *in vitro* development (F).

Because exogenous AA is toxic and rapidly sequestered into LDs, using it as Pxt substrate is challenging as we cannot target it specifically to the site of PG synthesis. However, we reasoned that

this toxicity could nevertheless be used as a tool to probe the functions of LDs and ATGL in regulating free AA levels.

Specifically, we investigated whether LD sequestration modulates AA toxicity. To be stored in LDs, free FAs must be incorporated into triglycerides. The final step of triglyceride synthesis is mediated by diacylglycerol O-acyl transferases (DGATs), which catalyze the attachment of a third FA to diacylglycerol. Like most animals, *Drosophila* encodes two such enzymes, DGAT1 (Midway) and DGAT2 (Yen et al., 2008). Genome-wide expression data indicate that DGAT1 predominates in most tissues, including in ovaries (Chintapalli et al., 2007). In *DGAT1* loss-of-function mutants, LDs fail to accumulate; these follicles die by S8/9 of oogenesis (Buszczak et al., 2002), although the underlying mechanism remains to be elucidated. If exogenous AA, as we hypothesize, is incorporated into LDs, then reducing DGAT1 levels should enhance AA toxicity (Fig. 7D). We tested this idea with our modified IVEM assay and treated follicles with 125 μM AA. At this concentration, 64% of wild-type follicles developed, whereas only 39% of *DGAT1*^{-/+} follicles developed (Fig. 7E). As exogenous AA is predominately incorporated into LDs (Fig. 7A-B'), these observations are consistent with the model that exogenous AA toxicity is reduced by sequestration into LDs.

If ATGL releases AA from internal LD stores and thus generates free AA, decreasing ATGL levels should reduce the toxicity of high levels of exogenous AA, as total free AA levels will be lower (Fig. 7D). Indeed, twofold more S10B follicles from *ATGL* heterozygotes developed in the presence of 500 μM AA than wild-type follicles (Fig. 7F). Together, these findings support the model that AA is stored in LDs and ATGL is required to release AA from LDs. This AA can then be used for PG production, and thus to promote the actin remodeling necessary for follicle development.

Pxt is not enriched on LDs

How does ATGL provide AA to Pxt for PG synthesis? PG production occurs at the cellular location of the COX enzyme, as the active site of the enzyme faces the lumen of the organelle it localizes to. In other systems, components of the PG synthesis machinery are sometimes enriched on LDs, and, therefore, PG production could occur on LDs (Bozza et al., 2011). To determine whether this is true during *Drosophila* oogenesis, we used immunostaining, LD purification, and *in vivo* centrifugation to assess Pxt's relationship to LDs in wild-type nurse cells. All three methods showed that Pxt is not enriched on LDs (Fig. 8). Immunostaining revealed that Pxt localizes to the Golgi compartments prior to S9 and to the endoplasmic reticulum (ER) by S10B, but not obviously to LDs (Fig. 8A-C'). Furthermore, Pxt localization was not affected by loss of ATGL (Fig. S6). We also prepared an LD-enriched biochemical fraction from ovary lysates, as previously described for embryos (Li et al., 2012), and analyzed it by western blotting for Pxt, PLIN2 (as a marker for LDs) and Calnexin (as marker for the ER). Pxt behaved like an ER protein, not like a LD protein (Fig. 8D,E). Finally, staining of fixed centrifuged follicles revealed no enrichment of Pxt in the LD layer (Fig. 8F-F'). We conclude that the majority of Pxt is not on LDs. Thus, strong enrichment of the PG synthesis machinery on LDs is not required for LDs to play a role in PG production.

Together, our data lead to the model that during S10B, AA stored in LD triglycerides is released by ATGL and serves as the substrate for PGF_{2α} production by ER-localized Pxt. PGF_{2α} signaling then drives the actin remodeling necessary for late-stage follicle development (Fig. 9).

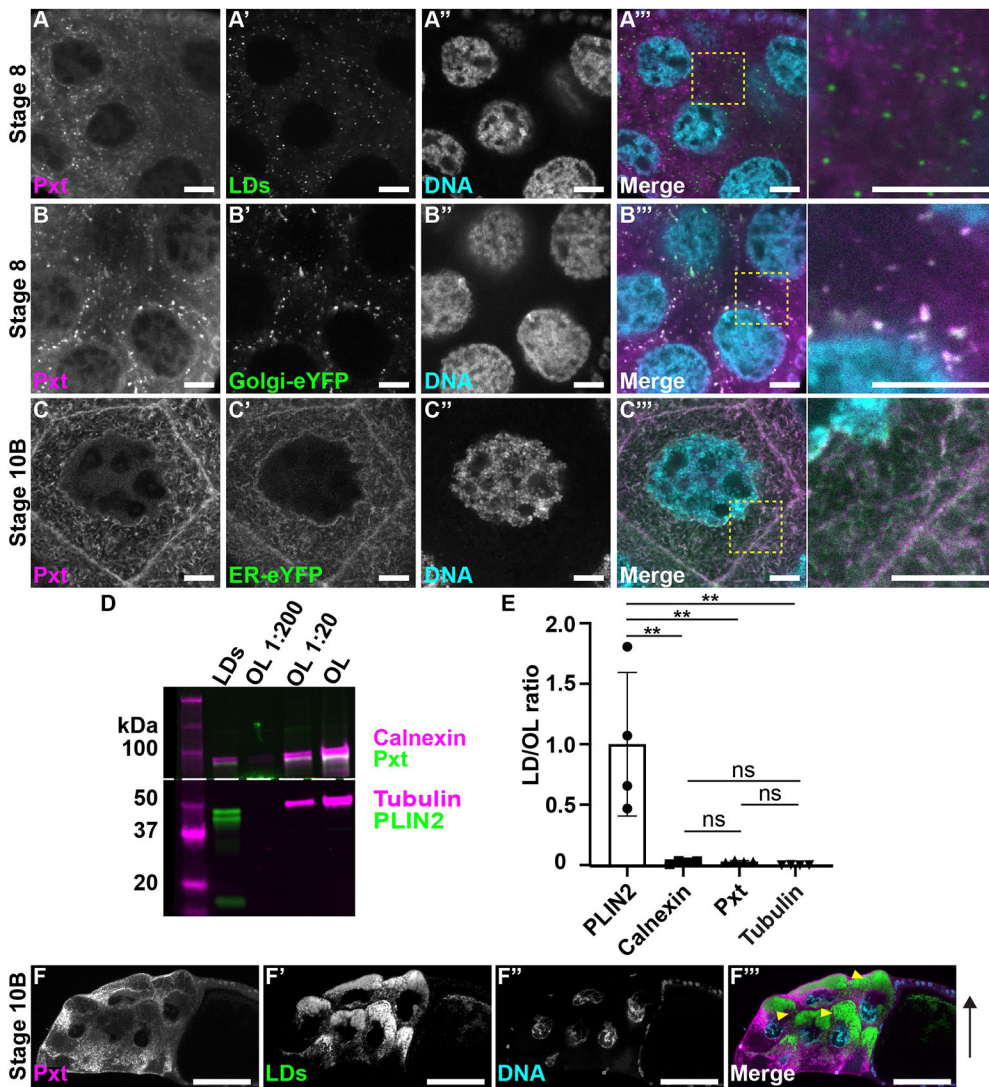


Fig. 8. Pxt is not enriched on lipid droplets. (A-C'') Confocal slice of wild-type (Oregon R) nurse cells of the indicated stages, stained for Pxt (A-C), organelle markers (A'-C') and DNA (A''-C''); Hoechst). Merged images (A'''-C'''); boxed regions are shown at higher magnification on the right): Pxt, magenta; organelle marker, green; DNA, cyan. Organelle marker: LDs (A-A''); Nile Red); Golgi-eYFP (B'-B''); and ER-eYFP (C'-C''). Scale bars: 10 μ m. (D) Western blots of LDs purified from whole ovaries and a dilution series of ovary lysate (OL) for Calnexin (magenta; ER marker) and Pxt (green) in the top half of the blot and α -Tubulin (magenta, loading control) and PLIN2 (green; LD marker) in the bottom half of the blot; dashed line indicates where the membrane was cut. (E) Quantification of protein abundance in the LD fraction relative to undiluted OL, normalized to the average value for PLIN2. Error bars represent s.d. ** $P=0.0028$, Tukey's multiple comparisons test. ns, not significant. (F-F'') Confocal slice of centrifuged wild-type Stage 10B follicle stained for Pxt (F, magenta), LDs (F', Nile Red, green), and DNA (F'', Hoechst, cyan). Orientation during centrifugation indicated by arrow. Arrowheads indicate the LD layer. Scale bars: 50 μ m. Pxt does not colocalize with LDs (A-A''), is not enriched on purified LDs (D,E), and does not co-accumulate with LDs in centrifuged follicles (F-F''). Instead, Pxt localizes to the Golgi during S8 (B-B'') and the ER during S10B (C-C'').

DISCUSSION

Our data reveal that the LDs produced during *Drosophila* oogenesis are not just lipid and protein stores for the future embryo, but play a

crucial regulatory role during follicle development. Loss of the triglyceride lipase ATGL results in cortical actin breakdown and defective actin bundle formation during S10B of oogenesis, an

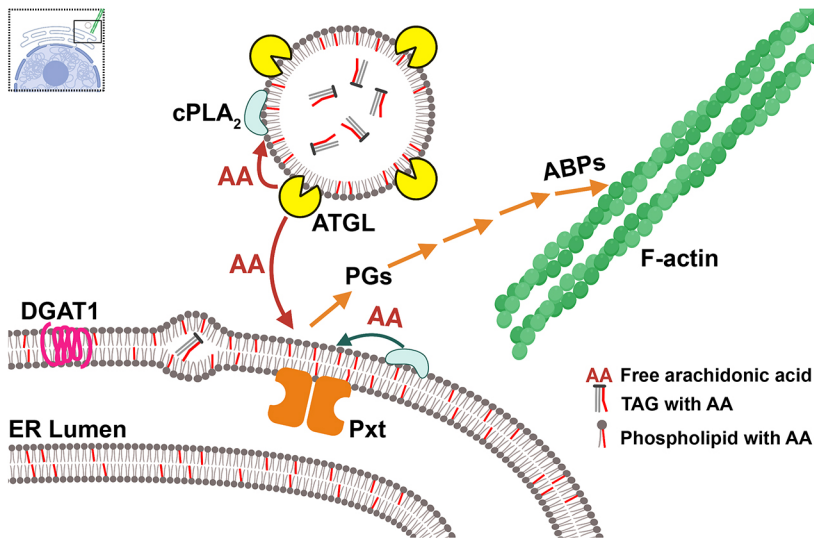


Fig. 9. ATGL regulates actin remodeling via prostaglandin signaling. Schematic (created with BioRender.com) summarizing our findings. TAG (triglyceride) synthesized by DGAT1 (magenta) accumulates between the leaflets of the ER membrane and LDs bud from the ER (not shown). AA (red lines) is stored in TAG or phospholipids. Our data lead to the model that ATGL (yellow) liberates AA from LD TAGs, providing AA, either directly or indirectly, for Pxt to produce PGs to regulate the activity of actin-binding proteins (ABPs), including Fascin and Enabled (not shown), to drive actin remodeling. AA (red) freed from TAG by ATGL may be directly supplied to Pxt or first incorporated into phospholipids on LDs, ER or other membranes. Subsequently, cPLA2 (light blue) releases AA from those phospholipids, providing AA for PG production.

unusual combination of phenotypes also observed in flies lacking Pxt, the *Drosophila* COX-like enzyme (Tootle and Spradling, 2008). Dominant genetic interactions and PG treatment of follicles *in vitro* reveal that ATGL and Pxt act in the same pathway to regulate actin remodeling, with ATGL upstream of Pxt. Our lipidomic, fluorescent AA, and AA toxicity studies support the model that AA is stored in triglycerides in LDs, ATGL is required to release that AA, which is then used as substrate for Pxt-dependent PG production, and those PGs regulate the actin dynamics necessary for follicle development (Fig. 9). Although PG signaling is known to regulate actin remodeling across organisms and cell types (Peppelenbosch et al., 1993; Pierce et al., 1999; Dormond et al., 2002; Tamma et al., 2003; Bulin et al., 2005; Birukova et al., 2007), this study provides the first evidence linking LDs to PG-dependent actin remodeling.

LDs provide the substrate for PG production

The enzymatic release of AA from cellular lipids is the rate-limiting step for PG production (Funk, 2001; Tootle, 2013). This free AA might originate from two different sources: phospholipids and triglycerides. In mammalian systems, both sources contribute to PG synthesis (Weller and Dvorak, 1994). Cytoplasmic phospholipase A2 (cPLA2) releases AA from phospholipids, and, in many cell types, inhibiting cPLA2 severely impairs PG production (Barbour and Dennis, 1993; Miyaura et al., 2003; Ghosh et al., 2004). Knockdown/inhibition of ATGL decreases PG production in mast cells (Dichlberger et al., 2014) and leukocytes (Schlager et al., 2015).

Our data support the model that in *Drosophila* follicles LD triglycerides are a source of AA for PG production and that ATGL is responsible for its release. AA from LDs might either directly serve as substrate for Pxt, or it might first be incorporated into phospholipids, to be subsequently released by cPLA2 (Fig. 9). Such models explain the genetic interaction between Pxt and ATGL (Figs 4 and 5A), the fact that exogenous PGF_{2α} can promote maturation of ATGL mutant follicles (Fig. 5B), the increase in AA-containing ovary triglycerides in ATGL mutants (Fig. 6G,H), and that reducing ATGL suppresses the lipotoxicity of exogenous AA (Fig. 7F). As the loss of Pxt causes more severe defects than the loss of ATGL, additional mechanisms of PG production likely exist. Perhaps ATGL and LDs initiates PG production that is later driven by cPLA2 or vice versa.

Site of PG synthesis

Although LDs are a source of AA during *Drosophila* oogenesis, our data do not identify the site of PG production. In some mammalian cell types, the PG synthesis machinery localizes to LDs and produces PGs there (Yu et al., 1998; Accioly et al., 2008; Moreira et al., 2009; Bozza et al., 2011; D'Avila et al., 2011). However, immunofluorescence and biochemical purification show that Pxt is not enriched on LDs, but is present throughout the ER during S10B (Fig. 8). How, then, do LDs facilitate PG production?

LDs originate from the ER and, in many cells, retain physical connections with the ER after biogenesis (Walther and Farese, 2012; Olzmann and Carvalho, 2019); in particular, the phospholipid monolayer around LDs can remain continuous with one leaflet of the ER membrane (Cottier and Schneider, 2022). Additional lipidic bridges between the ER and LDs can form transiently. These connections can mediate exchange of proteins and lipids (Salo et al., 2019; Cottier and Schneider, 2022; Olarte et al., 2022) and thus presumably transfer AA freed from LDs. What remains unclear is how far free AA can diffuse (either via the cytosol or within

membranes) before being metabolized; it might only be able to reach Pxt molecules present in ER regions immediately adjacent to LDs. Nevertheless, LD-derived AA could still reach distant regions of the ER by being incorporated into ER phospholipids, which can diffuse throughout the entire ER; in a second step, AA would then be released by cPLA2 to provide substrate for Pxt.

We find that LDs can function as important regulators of PG signaling even when the relevant COX enzyme are not enriched on LDs. This finding should prompt a careful re-examination of the functional impact of LDs in the many PG-producing cell types in which COX enzymes are distributed throughout the ER, nuclear envelope, and Golgi. Thus, LDs may regulate PG synthesis much more widely than previously recognized.

Why LDs?

If AA released from phospholipids can serve as substrate for Pxt, why is AA incorporated into LDs at all? Although LDs may store AA for later use in embryogenesis, our experiments raise the additional possibility that LDs are needed to buffer the toxicity of free AA. We found that high levels of exogenous AA inhibit follicle development (Fig. 7C), similar to previous observations in bovine granulosa cells where AA induces apoptosis (Zhang et al., 2019). In fact, AA is cytotoxic for many cells, e.g. cultured hippocampal neurons (Okuda et al., 1994), even at concentrations that overlap physiological ones (Pompeia et al., 2003). This toxicity is likely due to the diverse roles of AA in cellular signaling, even beyond PG synthesis (Brash, 2001; Tallima and El Ridi, 2018). Because of such toxicity, levels of free AA are tightly regulated across organisms, often by turning excess AA into inert triglycerides stored in LDs. Indeed, in mammalian cells, exogenous AA is initially almost exclusively incorporated into LDs (Weller and Dvorak, 1994; Bozza et al., 2009, 2011). LDs likely have a similar buffering role in *Drosophila* follicles, as exogenous fluorescent AA rapidly localizes to LDs (Fig. 7A-B') and triglyceride synthesis and breakdown modulate toxicity to exogenous AA (Fig. 7D-F).

Such an AA buffering function of LDs aligns with the recent recognition of LDs as a crucial way station during FA trafficking (Welte, 2015); they transiently sequester excess FAs from external and internal sources to prevent cellular damage, such as ER stress and mitochondrial dysfunction (Chitraju et al., 2017; Nguyen et al., 2017). Once safely stored in LDs, FAs can then be released in a regulated manner and directed to specific intracellular fates, such as energy production or signaling (Haemmerle et al., 2011; Rambold et al., 2015). Thus, LDs serve as FA trafficking hubs to both channel FAs to the correct intracellular destinations and buffer the FA supply.

ATGL functions in development

Like in mammals, ATGL in flies is best known for its role in fat storage and energy homeostasis in adipose tissue (Grönke et al., 2005). ATGL is highly expressed in the larval and adult fat body; its absence causes triglyceride overaccumulation in this tissue, and overexpression depletes organismal fat stores (Grönke et al., 2005). Here, we show that ATGL has a key role in follicle development, via PG signaling and actin remodeling. ATGL has previously been implicated in other important developmental transitions, although the underlying mechanisms remain unclear. In male flies, ATGL in neurons and testes regulates whole-body energy storage by an as-yet-uncharacterized mechanism thought to involve systemic signaling (Wat et al., 2020). In mammalian muscle, ATGL in satellite cells is important for proper differentiation and efficient recovery from muscle injury (Yue et al., 2022). Finally, ectopic

ATGL expression has beneficial roles in two *Drosophila* disease models: neurodegeneration due to mitochondrial dysfunction (Liu et al., 2015) and impairment of nephrocytes, components of the renal system, due to high-fat diet (Lubojevska et al., 2021). Our work identifies a specific signaling pathway, PG signaling, regulated by ATGL during oogenesis. It will be important to determine whether ATGL-based PG signaling facilitates the other developmental functions of ATGL.

LDs as regulators of female fertility

Animal development requires careful regulation of metabolism, specific to tissue type and developmental stage (Sieber and Spradling, 2017). Yet, despite the fact that LDs have a central role in lipid metabolism and energy homeostasis in normal physiology and diseases (Walther and Farese, 2012; Hashemi and Goodman, 2015; Welte, 2015), they have only been implicated as regulators of development in a handful of cases (Chan et al., 2007; Li et al., 2012; Johnson et al., 2018; Stephenson et al., 2021; Yue et al., 2022). Our analyses not only reveal that LDs play a crucial role during *Drosophila* follicle development, but also identify PG signaling as one mechanism whereby LDs act.

We speculate that this pathway is conserved across organisms. Indeed, LD accumulation, composition and localization are dynamic during oocyte maturation (Ami et al., 2011; Dunning et al., 2014), LDs are hubs for FA trafficking, and FA levels (including that of AA) are important for oocyte development in many species (Dunning et al., 2014; Prates et al., 2014; Brusentsev et al., 2019). Furthermore, in mouse models and in humans, metabolic syndrome causes failures in oocyte maturation and decreases fertility (Wattanakumtornkul et al., 2003; Jungheim et al., 2010; Cardozo et al., 2011; Marei et al., 2020). Obesity directly impairs oocyte quality, as fertilized oocytes from non-obese donors can be successfully transplanted into obese recipients without affecting implantation rates or pregnancy success (Styne-Gross et al., 2005). In addition, it is well-established that PG signaling plays key roles in oocyte development (Akil et al., 1996; Smith et al., 1996; Lim et al., 1997; Pall et al., 2001; Wang et al., 2004; Takahashi et al., 2006, 2010). Recent evidence also implicates LDs as foci of PG production during reproduction. COX enzymes localize to LDs in the rat corpus luteum (Arend et al., 2004), and in fetal membranes during advanced gestation and at induction of labor, times when PG synthesis and signaling are upregulated (Meadows et al., 2003, 2005). Whether the effects of PG on oogenesis and reproduction in mammals are due to changes in the actin cytoskeleton is not yet known. However, cytoplasmic actin density and cortical actin thickness increase during oocyte maturation, contribute to meiotic resumption, and play roles in fertilization and early embryonic divisions (Coticchio et al., 2015; Namgoong and Kim, 2016). Given these data, and our findings connecting LDs, PG signaling and actin remodeling during *Drosophila* oogenesis (Fig. 9), we speculate that this pathway is conserved across organisms to regulate oocyte development and contributes to infertility issues owing to limited or excess nutrition.

MATERIALS AND METHODS

Reagents and resources

See Table S2 for detailed information on the reagents used in these studies and Table S3 for the specific genotypes used in each figure/panel. All raw data used in this study can be found in Table S4.

Fly stocks

Flies used in actin quantification and IVEM experiments were maintained on cornmeal/agar/yeast food at room temperature except as noted below.

Flies used in all other experiments were maintained on molasses/agar/yeast/malt extract/corn flour/soy flour food at room temperature except as noted below. Stocks used were *y¹w¹* [Bloomington *Drosophila* Stock Center (BDSC), #1495], Oregon R (BDSC, #5), *bmm¹* (Grönke et al., 2003), *bmm-GFP* (BDSC, #94600, (Zhao et al., 2022), *pxt¹⁰¹⁰⁰* (Harvard Exelixis Collection; Thibault et al., 2004), *pxt^{EY03052}* (BDSC, #15620), *mdy^{QX25}* (BDSC, #5095), *Lsd-2^{KG00149}* (BDSC, #13382), *sqh-EYFP-ER* (BDSC, #7195; LaJeunesse et al., 2004), *sqh-EYFP-Golgi* (BDSC, #7193; LaJeunesse et al., 2004).

Immunofluorescence and fluorescent reagent staining

For Figs 1, 2, 7, 8, S4 and S5, the following method, referred to as Staining Method 1, was used. Adult female and male flies (to allow for mating) younger than 2 weeks old were fed dry yeast for 48 h at room temperature before ovary dissection in PBS-T (0.1% Triton X-100 in phosphate-buffered saline, PBS). Ovaries were fixed with 4.1% formaldehyde in PBS for 12 min at room temperature. Ovaries were washed with PBS-T, and follicles of desired stages were isolated using forceps and pin vises. Follicles were blocked in ovary block (10% bovine serum albumin, 0.1% Triton X-100, 0.02% sodium azide in PBS) overnight at 4°C. Primary antibodies were diluted in ovary block and incubated overnight at 4°C. The following primary antibodies were obtained from the Developmental Studies Hybridoma Bank (DSHB) developed under the auspices of the National Institute of Child Health and Human Development and maintained by the Department of Biology, University of Iowa (Iowa City, Iowa): mouse anti-Calnexin99A at 1:100 (Cnx99A 6-2-1, deposited by Munro, S.) and mouse anti-Golgin84 at 1:1000 (Golgin84 12-1, deposited by Munro, S.) (Riedel et al., 2016). Additionally, the following primary antibodies were used: rabbit anti-Pxt preabsorbed at 1:10 on *pxt^{-/-}* ovaries in ovary block and used at 1:1000 (Spracklen et al., 2014). GFP was visualized directly. Samples were washed three times with PBS-T, and then protected from light for the remainder of the experiment. Samples were incubated in the following secondary antibodies diluted to 1:1000 in ovary block overnight at 4°C: goat anti-rabbit IgG Alexa Fluor 633 (Invitrogen), goat anti-mouse IgG Alexa Fluor 488 (Invitrogen), and goat anti-rabbit IgG Alexa Fluor 488 (Invitrogen). Samples were washed three times with PBS-T and then stained with the following reagents diluted in ovary block: Phalloidin Alexa Fluor 633 (Invitrogen) 1:150, 1 h at room temperature; Nile Red (1 mg/ml, Sigma-Aldrich) 1:50, 1 h at room temperature; LipidSpot 610 (1000×, Biotium) 1:100, 20 min at room temperature and Hoechst 33342 (1 mg/ml, Thermo Fisher Scientific) 1:1000, 20 min at room temperature. Samples were washed three times with PBS-T, and then mounted on coverslips in Aqua Polymount (PolySciences).

For Figs 3, 4 and S1 the following protocol, referred to as Staining Method 2, was used. Adult female and male flies (to allow for mating) within 24 h of eclosion were fed wet yeast paste for 72 h at room temperature before dissection in room-temperature Grace's medium (Lonza). Ovaries were fixed in 4% paraformaldehyde in Grace's medium for 10 min at room temperature. Ovaries were washed six times (10 min each) in antibody wash (0.1% bovine serum albumin in PBS-T). Samples were stained overnight at 4°C with Alexa Fluor 488, 568, or 647 Phalloidin (Invitrogen) at 1:250. Samples were then washed five or six times in PBS-T for 10 min each and stained with 4'6'-diamidino-2-phenylindole (DAPI, 5 mg/ml) at 1:5000 in PBS for 10 min. Samples were rinsed in PBS and mounted in 1 mg/ml phenylenediamine in 50% glycerol, pH 9 (Platt and Michael, 1983).

Image acquisition and processing

Microscope images of fixed and stained *Drosophila* follicles were obtained using the following microscopes: Leica SPE confocal microscope with an ACS APO 20×/0.60 IMM CORR-/D or ACS APO 40×/1.5 oil CS objective (Leica Microsystems), Zeiss 700 confocal microscope or Zeiss 880 confocal microscope (Carl Zeiss Microscopy) using a Plan-Apochromat 20×/0.8 working distance (WD)=0.55 M27 objective, Zeiss 980 confocal microscope (Carl Zeiss Microscopy) using a Pln Apo 20×/0.8 or Pln Apo 40×/1.3 oil objective, or Leica SP5 confocal microscope (Leica Microsystems) using an HCX PL APO CS 63×/1.40 oil UV objective and Leica HyD detectors. Maximum projections of images, image cropping and image rotation were performed in Fiji/ImageJ software (Abramoff et al.,

2004); scale bars were added in either Fiji, Adobe Illustrator or Adobe Photoshop and figures were assembled using Adobe Illustrator. Images in Fig. 4 and Fig. S1 were brightened by 30% in Adobe Photoshop to improve visualization.

Quantification of actin defects

Confocal images of phalloidin-stained S10B follicles were collected as described. Actin bundle and cortical actin defects were scored by scanning through confocal z-stacks of S10B follicles in ImageJ by an operator unaware of the genotype. Representative images of follicles and scoring criteria are provided in Fig. S1. Briefly, actin bundles were scored as normal (score=0) if they were straight, forming from the nurse cell plasma membrane and oriented inwards toward the nurse cell nuclei. Mild defects in bundling (score=1) were defined as sparse bundle formation or slight delay in bundle growth relative to follicle development. Moderate defects (score=2) were defined as collapsed, thick and/or missing bundles from regions of the nurse cell plasma membrane. Severe defects (score=3) included those previously described, as well as a complete failure of bundles to form. Cortical actin was scored based on whether the cortical actin was intact or disrupted. Defects in cortical actin were evident by an absence or incomplete phalloidin staining between nurse cells and/or by nurse cell nuclei being in close proximity or contacting each other. Normal cortical actin (score=0) was defined as being completely intact and fully surrounding each nurse cell. The degree of severity of cortical actin defects was determined by the relative number of disruptions in cortical actin observed with mild defects (score=1) having a single instance, moderate defects (score=2) having two instances, and severe defects (score=3) having three or more instances of disrupted cortical actin. The ADI was then calculated by adding the bundle and cortical actin defect scores and binning them into normal (total score=0-1), mild defects (total score=2-3) or severe defects (score=4-6). Pearson's chi-squared analysis was performed using R (www.r-project.org).

IVEM assays

For both the standard IVEM and modified IVEM assays, adult female and male flies (to allow for mating) within 24 h of eclosion were fed wet yeast paste daily for 3 days prior to dissection. Ovaries were dissected in room temperature IVEM or modified IVEM medium. IVEM medium: Grace's medium (Lonza), 1× penicillin/streptomycin (from 100× stock, Gibco) and 10% FBS (Atlanta Biologicals). Modified IVEM medium: Grace's medium, 1× penicillin/streptomycin and 2.5% FBS. S10B follicles were isolated and distributed between wells of a 24-well plastic tissue culture plate (Falcon) and 1 ml of fresh medium was added with or without additions (described below). Follicles were incubated overnight at room temperature in the dark. The next day, the number of follicles at each developmental stage were counted, and the percentage developing was calculated; follicles that reached S12 and older were considered developed. Statistical analysis was performed using the unpaired *t*-test function in Prism 8 or 9 (GraphPad Software).

For the exogenous PGF_{2α} analog [Fluprostanol (Flu), Cayman Chemical Company] experiments, the standard IVEM was performed and stock solutions of 10 μM Flu and 0.5 M aspirin (Cayman Chemical Company) were prepared in 100% ethanol. For each genotype, there were two wells of S10B follicles with one well treated with ethanol (control) and the other with Flu (final concentration of 20 nM). As an additional control, wild-type follicles were also treated with 1.5 mM aspirin to verify that Flu rescues the loss of PG synthesis; any experiment in which Flu failed to suppress the effects of aspirin was excluded from the analysis. In all conditions, the total amount of ethanol was kept constant. Follicle development was assessed as described above.

For the exogenous fatty acid (AA or OA) experiments, the modified IVEM was performed. AA and OA stock solutions were made in 100% ethanol, and total ethanol volumes were kept constant in each experiment. Follicle development was assessed as described above.

Western blots

Follicles from well-fed females of the indicated genotypes and stage were dissected and fixed as described in Staining Method 1. Note that proteins from such samples ran at the same molecular weight as those from lysates prepared from live ovary tissue (Fig. S3). For each sample, 25-50 follicles

were collected and boiled in sample buffer (Laemmli Sample Buffer with 2-mercaptoethanol; both from Bio-Rad). Samples were run on 4-15% gradient gels (Bio-Rad) at 80-120 V and transferred onto PVDF membrane (Immobilon-FL, EMD Millipore) in Towbin (10% Tris-Glycine+20% methanol; 80 V for 30 min; for anti-PLIN2, anti-Pxt, anti-Calnexin) transfer buffer. Membranes were blocked for 1 h at room temperature in LI-COR Odyssey Block (LI-COR Biosciences). Membranes were incubated overnight at 4°C with primary antibodies diluted in Odyssey Block. The following primary antibodies were used: rabbit anti-Pxt (1:5000; Spracklen et al., 2014), rabbit anti-PLIN2 (1:5000; Welte et al., 2005), mouse anti-Calnexin99A (1:500, DSHB) and mouse anti-α-Tubulin (1:5000, Cell Signaling Technology). Membranes were washed three times in PBS-0.1% Tween 20 (PBS-Tween). The following secondary antibody incubations were performed for 1 h at room temperature: IRDye 800CW goat anti-rabbit IgG (1:5000, LI-COR), and IRDye 680RD goat anti-mouse IgG (1:5000, LI-COR). After secondary antibody incubation, membranes were washed twice in PBS-Tween and once in PBS. Membranes were imaged on a LI-COR Odyssey CLx imager and blots were processed and quantified in Image Studio Lite 5.2 (LI-COR). For quantifications, the fluorescence intensity of each band was measured and normalized to respective experimental controls. Data were analyzed and plotted using Prism (GraphPad).

Lipid extractions

Twenty-five ovaries per sample were dissected from mated, mixed-age, and dry yeast-fed females and homogenized in a 2 ml Eppendorf tube with a motorized pestle (KONTES pellet pestle) in PBS and kept on ice. Lysates were then incubated 1:1 in a 2:1 chloroform/methanol mixture overnight at 4°C. Samples were spun in an Eppendorf Microcentrifuge (model 5415D) at maximum speed at room temperature for 1 min, and the bottom organic layer was transferred to a 0.65 ml Eppendorf tube. Samples were then vacuum-dried and either analyzed immediately or stored at -80°C for thin layer chromatography analysis, or before being shipped on dry ice for mass spectrometry analysis.

Thin layer chromatography

Evaporated lipids were resuspended in 10 μl 2:1 chloroform/methanol and spotted on dehydrated silica plates (EMD Millipore; dehydrated by baking for 30 min at 100°C). Plates were placed in a chamber (Millipore Sigma/Sigma-Aldrich, Z266000) pre-saturated for 30 min with petroleum ether/diethyl ether/acetic acid (32:8:0.8) and allowed to develop until the solvent almost reached the top of the plates, and the solvent line was quickly marked with a pencil after removing plates from the chamber. The plates were then air-dried and briefly submerged in charring solution (50% ethanol, 3.2% H₂SO₄, 0.5% MgCl₂). Plates were air-dried briefly and were charred for 30 min at 120°C. Plates were imaged using a Bio-Rad Gel Doc and bands were quantified using Fiji. Lipids were identified according to Knittelfelder and Kohlwein (2017) and by comparing whole lipid extracts to lipid standards (Millipore Sigma). Colorimetric TAG band intensities were quantified in Fiji. Bands were normalized to one condition on the plate (e.g. WT, Fig. 6F) to account for variability in charring from plate to plate. Paired Student's *t*-tests were run in GraphPad Prism for Fig. 6F.

LC-MS/MS analysis

Extracted lipids were dissolved in corresponding volumes of 2:1 methanol: chloroform (v/v) and 5 μl of each sample was injected for positive and negative acquisition modes, respectively. Mobile phase A consisted of 3:2 (v/v) water/acetonitrile, including 10 mM ammonium formate and 0.1% formic acid, and mobile phase B consisted of 9:1 (v/v) 2-propanol/acetonitrile, also including 10 mM ammonium formate and 0.1% formic acid. Lipids were separated using an UltiMate 3000 UHPLC (Thermo Fisher Scientific) under a 90 min gradient; during 0-7 min, elution started with 40% B and increased to 55%; elution was then increased to 65% B from 7 to 8 min; maintained at 65% B from 8 to 12 min; increased to 70% B from 12 to 30 min; increased to 88% B from 30 to 31 min; increased to 95% B from 31 to 51 min; increased to 100% B from 51 to 53 min; maintained at 100% B during 53-73 min; then solvent B was decreased to 40% from 73 to 73.1 min, and then maintained for another 16.9 min for column

re-equilibration. The flow-rate was set to 0.2 ml/min. The column oven temperature was set to 55°C, and the temperature of the autosampler tray was set to 4°C. Eluted lipids were analyzed using Orbitrap Q Exactive (Thermo Fisher Scientific) Orbitrap mass analyzer. The spray voltage was set to 4.2 kV, and the heated capillary and the HESI were held at 320°C and 300°C, respectively. The S-lens RF level was set to 50, and the sheath and auxiliary gas were set to 35 and 3 units, respectively. These conditions were held constant for both positive and negative ionization mode acquisitions. External mass calibration was performed using the standard calibration mixture every 7 days. MS spectra of lipids were acquired in full-scan/data-dependent MS2 mode. For the full-scan acquisition, the resolution was set to 70,000, the AGC target was 1e6, the maximum integration time was 50 ms, and the scan range was $m/z=133.4-2000$. For data-dependent MS2, the top ten ions in each full scan were isolated with a 1.0 Da window, fragmented at a stepped normalized collision energy of 15, 25 and 35 units, and analyzed at a resolution of 17,500 with an AGC target of 2e5 and a maximum integration time of 100 ms. The underfill ratio was set to 0. The selection of the top ten ions was subject to isotopic exclusion with a dynamic exclusion window of 5.0 s. MS data were analyzed using LipidSearch version 4.1 SP (Thermo Fisher Scientific). Identified lipid species with grade A and B were manually curated. A total of 98 different triglyceride species were identified (Table S1).

For the quantitative analysis in Fig. 6A-D,G,H and Fig. S5, four biological replicates containing 25 ovaries each from both wild-type and *ATGL* mutant females were analyzed and the quantity of the 98 triglyceride species determined, relative to background. One wild-type sample contained an order of magnitude less lipid and was discarded as an outlier (Table S1). In total, 25 different types of FAs were identified in the ovary triglycerides. The abundance of each FA was estimated by summing the amount of each triglyceride species containing that FA, weighted by how many times that FA is represented in that triglyceride. For Fig. 6A,B, this abundance is expressed as fraction of the total amount of fatty acids such identified. For Fig. 6C, the signal for all species of phosphatidylcholine, phosphatidylethanolamine and phosphatidylinositol, respectively, was summed and normalized to the average of the wild type. For Fig. 6D, the signal for all triglyceride species was summed and normalized to the average of the wild type. To express the abundance of various lipid species relative to total lipids recovered (Fig. S5), values for various lipid species were divided by the sum of all lipids in the sample. For Fig. 6G,H, the signal for two AA-containing triglyceride species was computed and normalized to the average of the wild-type signal. Amounts and fractions were calculated using Microsoft Excel and graphed using Prism 8 (GraphPad Software). Statistical tests for Fig. 6 were as follows: 6A and 6C was Šidák's multiple comparisons test, 6B was Tukey's multiple comparisons test, 6D was an unpaired, two-tailed *t*-test, and 6G,H were unpaired, two-tailed *t*-tests.

Ovary centrifugation

Ovary centrifugations were performed as described (White and Welte, 2023), adapting a method previously described for embryos (Tran and Welte, 2010). Mated adult females of mixed ages fed dry yeast were anesthetized and beheaded before being mounted in microfuge tubes filled with 2.5% low melt agar. Tubes were spun for 10 min at 9000 *g* at 4°C. Flies were removed from agar with forceps and ovaries were isolated and fixed in 4% formaldehyde at room temperature for 15 min. Ovaries were washed three times in antibody wash for 5 min. Ovaries were stained with LipidSpot 610 (1000×, Biotium) 1:100 at room temperature for 20 min. Alternatively, ovaries incubated *in vitro* with fluorescently labeled AA were placed into the agar-filled microfuge tubes, covered with 10 μ l maturation medium (see below), and centrifuged for 10 min at ~6000 *g* at 4°C. Ovaries were recovered and treated as described in Staining Method 1. In the corresponding images, the orientation of centrifugation is indicated by an arrow that points towards the center of rotation.

Lipid droplet purification

For each replicate, 1000-1200 ovaries were rapidly dissected from mated and dry yeast-fed females and kept on ice in TSS (68 mM NaCl, 0.03% Triton X-100) in 2 ml Eppendorf tubes. Ovaries were then washed three

times with TKM (50 mM Tris, pH 7.4, 25 mM KCl, 5 mM MgCl₂) to remove detergent. TKM was removed and the volume of ovaries was estimated visually. Ovaries were kept on ice, to which were added: two times the estimated ovary volume of TKM+1 M sucrose, protease inhibitor cocktail to final concentration of 1× protease inhibitor cocktail (Sigma-Aldrich), and calyculin A serine/threonine phosphatase inhibitor (10 μ l per ml of volume; Cell Signaling Technology). Ovaries were homogenized on ice by grinding with an automated tissue grinder (KONTES pellet pestle) for 1-2 min, and then 20 μ l ovary lysate samples were transferred from the total lysate to 0.65 ml Eppendorf tubes and stored at -80°C. The remaining ovary lysates were spun at ~16,000 *g* for 10 min in an Eppendorf Microcentrifuge (model 5145D) at 4°C. The following was then added to samples slowly to avoid disturbing the LD layer: 300 μ l TKM+0.5 M sucrose, 300 μ l TKM+0.25 M sucrose, 400 μ l TKM (no sucrose). Tubes were spun for 20 min at 4°C, with the speed adjusted as follows: ~90 *g* for 5 min, ~2200 *g* for 5 min, ~16,000 *g* for 10 min. Purified LDs were then scooped off the top of the sucrose gradient using a drawn Pasteur pipette loop (Fisher Scientific, loop drawn by holding over a flame). LDs were washed off the pipette loop with 20 μ l TKM (no sucrose) and stored at -80°C until analyzed.

In previous western analyses, we loaded equal amounts of protein from LD preparations and original tissue lysate for easy comparison (Li et al., 2012). This approach was not feasible here because of the relatively low amounts of LDs recovered from the large volume of ovaries used. Instead, we compared the LD sample to dilutions of ovary lysate. Purified LDs and ovary lysates were diluted as indicated in 2× Laemmli Sample Buffer before being boiled for 30 min and subsequently run on 4-15% SDS-PAGE gradient gels (western blot protocol as described above). Before the blocking step, the membrane was cut with a razor blade between 50 and 75 kDa and each half was treated separately. Quantification was performed as described above in western blots.

Poly-D-lysine-coated dishes for live imaging

Poly-D-lysine (1 mg/ml, Gibco) was diluted 1:4 in PBS and 200 μ l was added to each glass-bottom culture dish (MatTek Corporation). Dishes were incubated at 37°C for 1 h, the excess liquid was removed, and the dishes were allowed to dry.

Fluorescent AA supplementation

A 2 mM chloroform/methanol stock solution of fluorescent AA {2-[(7-nitro-2-1,3-benzoxadiazol-4-yl)amino] AA (NBD AA), Avanti Polar Lipids} was kept at -80°C. Adult female and male flies (to allow for mating) younger than 2 weeks old were fed dry yeast for 48 h at room temperature or 24 h at 25°C in preparation for dissection. For *in vivo* supplementation, flies were fed supplemented yeast paste (1% sucrose, 5 μ M NBD AA, dry yeast) overnight and follicles were dissected, fixed and stained as described in Staining Method 1. For *in vitro* supplementation, ovaries were dissected in maturation medium [Schneider's *Drosophila* medium, Sigma-Aldrich; 15% FBS, Gibco; 10 mg/ml insulin, Sigma-Aldrich; 1× penicillin/streptomycin (10,000 U/ml penicillin and 10 mg/ml streptomycin, pH 6.95), Gibco], and then S10B follicles were isolated and incubated for 15 min in maturation medium supplemented with 5 μ M NBD AA and 2.5 μ l of LipidSpot 610 (1000×, Biotium). The medium was removed by aspiration and the follicles were washed once in fresh maturation medium for 5 min. The follicles were then transferred to a poly-D-lysine-coated, glass-bottom culture dish with 200 μ l of maturation medium. Follicles were allowed to adhere to the culture dish for 5 min prior to imaging.

Acknowledgements

We thank the Dunnwald lab for helpful discussions, and Dr Martine Dunnwald, the Tootle lab and the Welte lab for helpful discussions and careful review of the manuscript. We are grateful to Marcus Kilwein for help with thin layer chromatography. The Harvard T. H. Chan Advanced Multi-omics Platform at the Harvard T. H. Chan School of Public Health performed the lipidomics analysis. We thank Xun Huang for the gift of the bmm-GFP fly stocks. Stocks obtained from the Bloomington *Drosophila* Stock Center (NIH P40OD018537) were used in this study. At the University of Iowa, Information Technology Services – Research Services provided data storage support.

Competing interests

The authors declare no competing or financial interests.

Author contributions

Conceptualization: M.S.G., J.M.T., T.L.T., M.A.W.; Methodology: M.S.G., J.M.T., R.P.W., M.R.J., Z.W.L., T.L.T., M.A.W.; Formal analysis: M.S.G., J.M.T., R.P.W., M.R.J., Z.W.L.; Investigation: M.S.G., J.M.T.; Writing - original draft: M.S.G., J.M.T., T.L.T., M.A.W.; Writing - review & editing: M.S.G., J.M.T., R.P.W., M.R.J., Z.W.L., T.L.T., M.A.W.; Visualization: M.S.G., J.M.T.; Supervision: T.L.T., M.A.W.; Project administration: T.L.T., M.A.W.; Funding acquisition: T.L.T., M.A.W.

Funding

This project is supported by the National Institutes of Health (GM116885 and GM144057 to T.L.T., GM102155 to M.A.W.), as well as a PumpPrimerII grant from the University of Rochester (M.A.W.). M.S.G. is supported by National Institutes of Health grant T32 CA078586 Free Radical and Radiation Biology, University of Iowa. Open Access funding provided by The University of Iowa. Deposited in PMC for immediate release.

Data availability

All relevant data can be found within the article and its supplementary information.

Peer review history

The peer review history is available online at <https://journals.biologists.com/dev/lookup/doi/10.1242/dev.201516.reviewer-comments.pdf>.

References

- Abramoff, M., Magalhaes, P. and Ram, S.** (2004). Image processing with ImageJ. *Biophotonics Int.* **11**, 36-42.
- Accioly, M. T., Pacheco, P., Maya-Monteiro, C. M., Carrossini, N., Robbs, B. K., Oliveira, S. S., Kaufmann, C., Morgado-Diaz, J. A., Bozza, P. T. and Viola, J. P.** (2008). Lipid bodies are reservoirs of cyclooxygenase-2 and sites of prostaglandin-E2 synthesis in colon cancer cells. *Cancer Res.* **68**, 1732-1740. doi:10.1158/0008-5472.CAN-07-1999
- Akil, M., Amos, R. S. and Stewart, P.** (1996). Infertility may sometimes be associated with NSAID consumption. *Br. J. Rheumatol.* **35**, 76-78. doi:10.1093/rheumatology/35.1.76
- Ami, D., Mereghetti, P., Natalello, A., Doglia, S. M., Zanoni, M., Redi, C. A. and Monti, M.** (2011). FTIR spectral signatures of mouse antral oocytes: molecular markers of oocyte maturation and developmental competence. *Biochim. Biophys. Acta* **1813**, 1220-1229. doi:10.1016/j.bbamer.2011.03.009
- Arend, A., Masso, R., Masso, M. and Selstam, G.** (2004). Electron microscope immunocytochemical localization of cyclooxygenase-1 and -2 in pseudopregnant rat corpus luteum during luteolysis. *Prostaglandins Other Lipid Mediat.* **74**, 1-10. doi:10.1016/j.prostaglandins.2004.05.002
- Barbour, S. E. and Dennis, E. A.** (1993). Antisense inhibition of group II phospholipase A2 expression blocks the production of prostaglandin E2 by P388D1 cells. *J. Biol. Chem.* **268**, 21875-21882. doi:10.1016/S0021-9258(20)80622-X
- Bersuker, K., Peterson, C. W. H., To, M., Sahl, S. J., Savikhin, V., Grossman, E. A., Nomura, D. K. and Olzmann, J. A.** (2018). A proximity labeling strategy provides insights into the composition and dynamics of lipid droplet proteomes. *Dev. Cell* **44**, 97-112.e117. doi:10.1016/j.devcel.2017.11.020
- Birukova, A. A., Zagranichnaya, T., Fu, P., Alekseeva, E., Chen, W., Jacobson, J. R. and Birukov, K. G.** (2007). Prostaglandins PGE(2) and PG(I2) promote endothelial barrier enhancement via PKA- and Epac1/Rap1-dependent Rac activation. *Exp. Cell Res.* **313**, 2504-2520. doi:10.1016/j.yexcr.2007.03.036
- Bozza, P. T., Magalhaes, K. G. and Weller, P. F.** (2009). Leukocyte lipid bodies - Biogenesis and functions in inflammation. *Biochim. Biophys. Acta* **1791**, 540-551. doi:10.1016/j.bbaliip.2009.01.005
- Bozza, P. T., Bakker-Abreu, I., Navarro-Xavier, R. A. and Bandeira-Melo, C.** (2011). Lipid body function in eicosanoid synthesis: an update. *Prostaglandins Leukot. Essent. Fatty Acids* **85**, 205-213. doi:10.1016/j.plefa.2011.04.020
- Brash, A. R.** (2001). Arachidonic acid as a bioactive molecule. *J. Clin. Invest.* **107**, 1339-1345. doi:10.1172/JCI13210
- Brusentsev, E. Y., Mokrousova, V. I., Igonina, T. N., Rozhkova, I. N. and Amstislavsky, S. Y.** (2019). Role of lipid droplets in the development of oocytes and preimplantation embryos in mammals. *Russian J. Dev. Biol.* **50**, 230-237. doi:10.1134/S1062360419050102
- Bulin, C., Albrecht, U., Bode, J. G., Weber, A. A., Schrör, K., Levkau, B. and Fischer, J. W.** (2005). Differential effects of vasodilatory prostaglandins on focal adhesions, cytoskeletal architecture, and migration in human aortic smooth muscle cells. *Arterioscler. Thromb. Vasc. Biol.* **25**, 84-89. doi:10.1161/01.ATV.0000146814.81581.68
- Buszczak, M. and Cooley, L.** (2000). Eggs to die for: cell death during Drosophila oogenesis. *Cell Death Differ.* **7**, 1071-1074. doi:10.1038/sj.cdd.4400755
- Buszczak, M., Lu, X., Segraves, W. A., Chang, T. Y. and Cooley, L.** (2002). Mutations in the midway gene disrupt a Drosophila acyl coenzyme A: diacylglycerol acyltransferase. *Genetics* **160**, 1511-1518. doi:10.1093/genetics/160.4.1511
- Cardozo, E., Pavone, M. E. and Hirshfeld-Cytron, J. E.** (2011). Metabolic syndrome and oocyte quality. *Trends Endocrinol. Metab.* **22**, 103-109. doi:10.1016/j.tem.2010.12.002
- Cermelli, S., Guo, Y., Gross, S. P. and Welte, M. A.** (2006). The lipid-droplet proteome reveals that droplets are a protein-storage depot. *Curr. Biol.* **16**, 1783-1795. doi:10.1016/j.cub.2006.07.062
- Chan, A. P., Kloc, M., Larabell, C. A., Legros, M. and Etkin, L. D.** (2007). The maternally localized RNA fatvg is required for cortical rotation and germ cell formation. *Mech. Dev.* **124**, 350-363. doi:10.1016/j.mod.2007.02.001
- Chintapalli, V. R., Wang, J. and Dow, J. A. T.** (2007). Using FlyAtlas to identify better Drosophila melanogaster models of human disease. *Nat. Genet.* **39**, 715-720. doi:10.1038/ng2049
- Chitruju, C., Mejhert, N., Haas, J. T., Diaz-Ramirez, L. G., Grueter, C. A., Imbriglio, J. E., Pinto, S., Koliwad, S. K., Walther, T. C. and Farese, R. V., Jr.** (2017). Triglyceride synthesis by DGAT1 protects adipocytes from lipid-induced ER stress during lipolysis. *Cell Metab.* **26**, 407-418.e403. doi:10.1016/j.cmet.2017.07.012
- Coticchio, G., Dal Canto, M., Mignini Renzini, M., Guglielmo, M. C., Brambillasca, F., Turchi, D., Novara, P. V. and Fadini, R.** (2015). Oocyte maturation: gamete-somatic cells interactions, meiotic resumption, cytoskeletal dynamics and cytoplasmic reorganization. *Hum. Reprod. Update* **21**, 427-454. doi:10.1093/humupd/dmv011
- Cottier, S. and Schneider, R.** (2022). Lipid droplets form a network interconnected by the endoplasmic reticulum through which their proteins equilibrate. *J. Cell Sci.* **135**, jcs258819. doi:10.1242/jcs.258819
- D'Avila, H., Freire-De-Lima, C. G., Roque, N. R., Teixeira, L., Barja-Fidalgo, C., Silva, A. R., Melo, R. C. N., Dosreis, G. A., Castro-Faria-Neto, H. C. and Bozza, P. T.** (2011). Host cell lipid bodies triggered by Trypanosoma cruzi infection and enhanced by the uptake of apoptotic cells are associated with prostaglandin E(2) generation and increased parasite growth. *J. Infect. Dis.* **204**, 951-961. doi:10.1093/infdis/jir432
- Dichlberger, A., Schlager, S., Maaninka, K., Schneider, W. J. and Kovanen, P. T.** (2014). Adipose triglyceride lipase regulates eicosanoid production in activated human mast cells. *J. Lipid Res.* **55**, 2471-2478. doi:10.1194/jlr.M048553
- Dormond, O., Bezzi, M., Mariotti, A. and Rüegg, C.** (2002). Prostaglandin E2 promotes integrin alpha Vbeta 3-dependent endothelial cell adhesion, rac-activation, and spreading through cAMP/PKA-dependent signaling. *J. Biol. Chem.* **277**, 45838-45846. doi:10.1074/jbc.M209213200
- Dunning, K. R., Cashman, K., Russell, D. L., Thompson, J. G., Norman, R. J. and Robker, R. L.** (2010). Beta-oxidation is essential for mouse oocyte developmental competence and early embryo development. *Biol. Reprod.* **83**, 909-918. doi:10.1095/biolreprod.110.084145
- Dunning, K. R., Akison, L. K., Russell, D. L., Norman, R. J. and Robker, R. L.** (2011). Increased beta-oxidation and improved oocyte developmental competence in response to l-carnitine during ovarian in vitro follicle development in mice. *Biol. Reprod.* **85**, 548-555. doi:10.1095/biolreprod.110.090415
- Dunning, K. R., Russell, D. L. and Robker, R. L.** (2014). Lipids and oocyte developmental competence: the role of fatty acids and beta-oxidation. *Reproduction* **148**, R15-R27. doi:10.1530/REP-13-0251
- Funk, C. D.** (2001). Prostaglandins and leukotrienes: advances in eicosanoid biology. *Science* **294**, 1871-1875. doi:10.1126/science.294.5548.1871
- Ghosh, M., Stewart, A., Tucker, D. E., Bonventre, J. V., Murphy, R. C. and Leslie, C. C.** (2004). Role of cytosolic phospholipase A(2) in prostaglandin E(2) production by lung fibroblasts. *Am. J. Respir. Cell Mol. Biol.* **30**, 91-100. doi:10.1165/rcmb.2003-0005OC
- Groen, C. M., Spracklen, A. J., Fagan, T. N. and Tootle, T. L.** (2012). Drosophila Fascin is a novel downstream target of prostaglandin signaling during actin remodeling. *Mol. Biol. Cell* **23**, 4567-4578. doi:10.1091/mbc.e12-05-0417
- Grönke, S., Beller, M., Fellert, S., Ramakrishnan, H., Jäckle, H. and Kühnlein, R. P.** (2003). Control of fat storage by a Drosophila PAT domain protein. *Curr. Biol.* **13**, 603-606. doi:10.1016/S0960-9822(03)00175-1
- Grönke, S., Mildner, A., Fellert, S., Tennagels, N., Petry, S., Müller, G., Jäckle, H. and Kühnlein, R. P.** (2005). Brummer lipase is an evolutionary conserved fat storage regulator in Drosophila. *Cell Metab.* **1**, 323-330. doi:10.1016/j.cmet.2005.04.003
- Guild, G. M., Connelly, P. S., Shaw, M. K. and Tilney, L. G.** (1997). Actin filament cables in Drosophila nurse cells are composed of modules that slide passively past one another during dumping. *J. Cell Biol.* **138**, 783-797. doi:10.1083/jcb.138.4.783
- Haemmerle, G., Moustafa, T., Woelkart, G., Büttner, S., Schmidt, A., Van De Weijer, T., Hesselink, M., Jaeger, D., Kiensberger, P. C., Zierler, K. et al.** (2011). ATGL-mediated fat catabolism regulates cardiac mitochondrial function via PPAR-alpha and PGC-1. *Nat. Med.* **17**, 1076-1085. doi:10.1038/nm.2439
- Hashemi, H. F. and Goodman, J. M.** (2015). The life cycle of lipid droplets. *Curr. Opin. Cell Biol.* **33**, 119-124. doi:10.1016/j.cob.2015.02.002

- Huelsmann, S., Yläñne, J. and Brown, N. H. (2013). Filopodia-like actin cables position nuclei in association with perinuclear actin in *Drosophila* nurse cells. *Dev. Cell* **26**, 604–615. doi:10.1016/j.devcel.2013.08.014
- Jambor, H., Surendranath, V., Kalinka, A. T., Mejsstrik, P., Saalfeld, S. and Tomancak, P. (2015). Systematic imaging reveals features and changing localization of mRNAs in *Drosophila* development. *eLife* **4**, e05003. doi:10.7554/eLife.05003
- Johnson, M. R., Stephenson, R. A., Ghaemmaghami, S. and Welte, M. A. (2018). Developmentally regulated H2Av buffering via dynamic sequestration to lipid droplets in *Drosophila* embryos. *eLife* **7**, e36021. doi:10.7554/eLife.36021
- Jungheim, E. S., Schoeller, E. L., Marquard, K. L., Louden, E. D., Schaffer, J. E. and Moley, K. H. (2010). Diet-induced obesity model: abnormal oocytes and persistent growth abnormalities in the offspring. *Endocrinology* **151**, 4039–4046. doi:10.1210/en.2010-0098
- Knittelfelder, O. L. and Kohlwein, S. D. (2017). Thin-layer chromatography to separate phospholipids and neutral lipids from yeast. *Cold Spring Harb. Protoc.* **2017**. doi:10.1101/pdb.prot085456
- Lajeunesse, D. R., Buckner, S. M., Lake, J., Na, C., Pirt, A. and Fromson, K. (2004). Three new *Drosophila* markers of intracellular membranes. *BioTechniques* **36**, 784–788, 790. doi:10.2144/04365ST01
- Li, Z., Thiel, K., Thul, P. J., Beller, M., Kühnlein, R. P. and Welte, M. A. (2012). Lipid droplets control the maternal histone supply of *Drosophila* embryos. *Curr. Biol.* **22**, 2104–2113. doi:10.1016/j.cub.2012.09.018
- Lim, H., Paria, B. C., Das, S. K., Dinchuk, J. E., Langenbach, R., Trzaskos, J. M. and Dey, S. K. (1997). Multiple female reproductive failures in cyclooxygenase 2-deficient mice. *Cell* **91**, 197–208. doi:10.1016/S0092-8674(00)80402-X
- Liu, L., Zhang, K., Sandoval, H., Yamamoto, S., Jaiswal, M., Sanz, E., Li, Z., Hui, J., Graham, B. H., Quintana, A. et al. (2015). Glial lipid droplets and ROS induced by mitochondrial defects promote neurodegeneration. *Cell* **160**, 177–190. doi:10.1016/j.cell.2014.12.019
- Lubojska, A., Stefana, M. I., Sorge, S., Bailey, A. P., Lampe, L., Yoshimura, A., Burrell, A., Collinson, L. and Gould, A. P. (2021). Adipose triglyceride lipase protects renal cell endocytosis in a *Drosophila* dietary model of chronic kidney disease. *PLoS Biol.* **19**, e3001230. doi:10.1371/journal.pbio.3001230
- Marei, W. F. A., Smits, A., Mohey-Elsaeed, O., Pintelon, I., Ginneberge, D., Bols, P. E. J., Moerloose, K. and Leroy, J. (2020). Differential effects of high fat diet-induced obesity on oocyte mitochondrial functions in inbred and outbred mice. *Sci. Rep.* **10**, 9806. doi:10.1038/s41598-020-66702-6
- Meadows, J. W., Eis, A. L. W., Brockman, D. E. and Myatt, L. (2003). Expression and localization of prostaglandin synthase isoforms in human fetal membranes in term and preterm labor. *J. Clin. Endocrinol. Metab.* **88**, 433–439. doi:10.1210/jc.2002-021061
- Meadows, J. W., Pitzer, B., Brockman, D. E. and Myatt, L. (2005). Expression and localization of adipophilin and perilipin in human fetal membranes: association with lipid bodies and enzymes involved in prostaglandin synthesis. *J. Clin. Endocrinol. Metab.* **90**, 2344–2350. doi:10.1210/jc.2004-1199
- Miyaura, C., Inada, M., Matsumoto, C., Ohshiba, T., Uozumi, N., Shimizu, T. and Ito, A. (2003). An essential role of cytosolic phospholipase A2 α in prostaglandin E $_2$ -mediated bone resorption associated with inflammation. *J. Exp. Med.* **197**, 1303–1310. doi:10.1084/jem.20030015
- Moreira, L. S., Piva, B., Gentile, L. B., Mesquita-Santos, F. P., D'Avila, H., Maya-Monteiro, C. M., Bozza, P. T., Bandeira-Melo, C. and Diaz, B. L. (2009). Cytosolic phospholipase A2-driven PGE2 synthesis within unsaturated fatty acids-induced lipid bodies of epithelial cells. *Biochim. Biophys. Acta* **1791**, 156–165. doi:10.1016/j.bbalip.2009.01.003
- Namgoong, S. and Kim, N.-H. (2016). Roles of actin binding proteins in mammalian oocyte maturation and beyond. *Cell Cycle* **15**, 1830–1843. doi:10.1080/15384101.2016.1181239
- Nguyen, T. B., Louie, S. M., Daniele, J. R., Tran, Q., Dillin, A., Zoncu, R., Nomura, D. K. and Olzmann, J. A. (2017). DGAT1-dependent lipid droplet biogenesis protects mitochondrial function during starvation-induced autophagy. *Dev. Cell* **42**, 9–21.e25. doi:10.1016/j.devcel.2017.06.003
- Okuda, S., Saito, H. and Katsuki, H. (1994). Arachidonic acid: toxic and trophic effects on cultured hippocampal neurons. *Neuroscience* **63**, 691–699. doi:10.1016/0306-4522(94)90515-0
- Olarte, M.-J., Swanson, J. M. J., Walther, T. C. and Farese, R. V., Jr. (2022). The CYTOLD and ERTOLD pathways for lipid droplet-protein targeting. *Trends Biochem. Sci.* **47**, 39–51. doi:10.1016/j.tibs.2021.08.007
- Olzmann, J. A. and Carvalho, P. (2019). Dynamics and functions of lipid droplets. *Nat. Rev. Mol. Cell Biol.* **20**, 137–155. doi:10.1038/s41580-018-0085-z
- Pall, M., Friden, B. E. and Brannstrom, M. (2001). Induction of delayed follicular rupture in the human by the selective COX-2 inhibitor rofecoxib: a randomized double-blind study. *Hum. Reprod.* **16**, 1323–1328. doi:10.1093/humrep/16.7.1323
- Parra-Peralbo, E. and Culi, J. (2011). *Drosophila* lipophorin receptors mediate the uptake of neutral lipids in oocytes and imaginal disc cells by an endocytosis-independent mechanism. *PLoS Genet.* **7**, e1001297. doi:10.1371/journal.pgen.1001297
- Peppelenbosch, M. P., Tertoolen, L. G. J., Hage, W. J. and de Laat, S. W. (1993). Epidermal growth factor-induced actin remodeling is regulated by 5-lipoxygenase and cyclooxygenase products. *Cell* **74**, 565–575. doi:10.1016/0092-8674(93)80057-L
- Pfisterer, S. G., Gateva, G., Horvath, P., Pirhonen, J., Salo, V. T., Karhinen, L., Varjosalo, M., Ryhänen, S. J., Lappalainen, P. and Ikonen, E. (2017). Role for formin-like 1-dependent acto-myosin assembly in lipid droplet dynamics and lipid storage. *Nat. Commun.* **8**, 14858. doi:10.1038/ncomms14858
- Pierce, K. L., Fujino, H., Srinivasan, D. and Regan, J. W. (1999). Activation of FP prostanoid receptor isoforms leads to Rho-mediated changes in cell morphology and in the cell cytoskeleton. *J. Biol. Chem.* **274**, 35944–35949. doi:10.1074/jbc.274.50.35944
- Platt, J. L. and Michael, A. F. (1983). Retardation of fading and enhancement of intensity of immunofluorescence by p-phenylenediamine. *J. Histochem. Cytochem.* **31**, 840–842. doi:10.1177/31.6.6341464
- Pompeia, C., Lima, T. and Curi, R. (2003). Arachidonic acid cytotoxicity: can arachidonic acid be a physiological mediator of cell death? *Cell Biochem. Funct.* **21**, 97–104. doi:10.1002/cbf.1012
- Prates, E. G., Nunes, J. T. and Pereira, R. M. (2014). A role of lipid metabolism during cumulus-oocyte complex maturation: impact of lipid modulators to improve embryo production. *Mediators Inflamm.* **2014**, 692067. doi:10.1155/2014/692067
- Rambold, A. S., Cohen, S. and Lippincott-Schwartz, J. (2015). Fatty acid trafficking in starved cells: regulation by lipid droplet lipolysis, autophagy, and mitochondrial fusion dynamics. *Dev. Cell* **32**, 678–692. doi:10.1016/j.devcel.2015.01.029
- Riedel, F., Gillingham, A. K., Rosa-Ferreira, C., Galindo, A. and Munro, S. (2016). An antibody toolkit for the study of membrane traffic in *Drosophila* melanogaster. *Biol. Open* **5**, 987–992. doi:10.1242/bio.018937
- Salo, V. T., Li, S., Vihinen, H., Hölttä-Vuori, M., Szkalitsy, A., Horvath, P., Belevich, I., Peränen, J., Thiele, C., Somerharju, P. et al. (2019). Seipin facilitates triglyceride flow to lipid droplet and counteracts droplet ripening via endoplasmic reticulum contact. *Dev. Cell* **50**, 478–493.e479. doi:10.1016/j.devcel.2019.05.016
- Schlager, S., Goeritzer, M., Jandl, K., Frei, R., Vujic, N., Kolb, D., Strohmaier, H., Dorow, J., Eichmann, T. O., Rosenberger, A. et al. (2015). Adipose triglyceride lipase acts on neutrophil lipid droplets to regulate substrate availability for lipid mediator synthesis. *J. Leukoc. Biol.* **98**, 837–850. doi:10.1189/jlb.3A0515-206R
- Shen, L. R., Lai, C. Q., Feng, X., Parnell, L. D., Wan, J. B., Wang, J. D., Li, D., Ordovas, J. M. and Kang, J. X. (2010). *Drosophila* lacks C20 and C22 PUFAs. *J. Lipid Res.* **51**, 2985–2992. doi:10.1194/jlr.M008524
- Sieber, M. H. and Spradling, A. C. (2017). The role of metabolic states in development and disease. *Curr. Opin. Genet. Dev.* **45**, 58–68. doi:10.1016/j.gde.2017.03.002
- Smith, G., Roberts, R., Hall, C. and Nuki, G. (1996). Reversible ovulatory failure associated with the development of luteinized unruptured follicles in women with inflammatory arthritis taking non-steroidal anti-inflammatory drugs. *Br. J. Rheumatol.* **35**, 458–462. doi:10.1093/rheumatology/35.5.458
- Spracklen, A. J. and Tootle, T. L. (2013). The utility of stage-specific mid-to-late *Drosophila* follicle isolation. *J. Vis. Exp.* **82**, 50493. doi:10.3791/50493-v
- Spracklen, A. J. and Tootle, T. L. (2015). *Drosophila* – a model for studying prostaglandin signaling. In: *Bioactive Lipid Mediators: Current Reviews and Protocols* (ed. T. Yokomizo and M. Murakami), pp. 181–197. Springer Protocols.
- Spracklen, A. J., Kelsch, D. J., Chen, X., Spracklen, C. N. and Tootle, T. L. (2014). Prostaglandins temporally regulate cytoplasmic actin bundle formation during *Drosophila* oogenesis. *Mol. Biol. Cell* **25**, 397–411. doi:10.1091/mbc.e13-07-0366
- Spracklen, A. J., Lamb, M. C., Groen, C. M. and Tootle, T. L. (2019). Pharmacogenetic screen to uncover actin regulators targeted by prostaglandins during *Drosophila* oogenesis. *G3 (Bethesda)* **9**, 3555–3565. doi:10.1534/g3.119.400704
- Stephenson, R. A., Thomalla, J. M., Chen, L., Kolkhof, P., White, R. P., Beller, M. and Welte, M. A. (2021). Sequestration to lipid droplets promotes histone availability by preventing turnover of excess histones. *Development* **148**, dev199381. doi:10.1242/dev.199381
- Styne-Gross, A., Elkind-Hirsch, K. and Scott, R. T., Jr. (2005). Obesity does not impact implantation rates or pregnancy outcome in women attempting conception through oocyte donation. *Fertil. Steril.* **83**, 1629–1634. doi:10.1016/j.fertnstert.2005.01.099
- Sugimoto, Y., Inazumi, T. and Tsuchiya, S. (2015). Roles of prostaglandin receptors in female reproduction. *J. Biochem.* **157**, 73–80. doi:10.1093/jb/mvu081
- Sun, H., Gong, T.-T., Jiang, Y.-T., Zhang, S., Zhao, Y.-H. and Wu, Q.-J. (2019). Global, regional, and national prevalence and disability-adjusted life-years for infertility in 195 countries and territories, 1990–2017: results from a global burden of disease study, 2017. *Aging (Albany NY)* **11**, 10952–10991. doi:10.18632/aging.102497
- Takahashi, T., Morrow, J. D., Wang, H. and Dey, S. K. (2006). Cyclooxygenase-2-derived prostaglandin E(2) directs oocyte maturation by differentially influencing multiple signaling pathways. *J. Biol. Chem.* **281**, 37117–37129. doi:10.1074/jbc.M608202200
- Takahashi, T., Igarashi, H., Amita, M., Hara, S. and Kurachi, H. (2010). Roles of prostaglandins during oocyte maturation: lessons from knockout mice. *J. Mammal. Ova Res.* **27**, 11–20. doi:10.1274/jmor.27.11

- Tallima, H. and El Ridi, R. (2018). Arachidonic acid: Physiological roles and potential health benefits - a review. *J. Adv. Res.* **11**, 33-41. doi:10.1016/j.jare.2017.11.004
- Tamma, G., Wiesner, B., Furkert, J., Hahm, D., Oksche, A., Schaefer, M., Valenti, G., Rosenthal, W. and Klussmann, E. (2003). The prostaglandin E2 analogue sulprostone antagonizes vasopressin-induced antidiuresis through activation of Rho. *J. Cell Sci.* **116**, 3285-3294. doi:10.1242/jcs.00640
- Tan, Y., Jin, Y., Zhao, P., Wu, J. and Ren, Z. (2021). Lipid droplets contribute myogenic differentiation in C2C12 by promoting the remodeling of the actin-filament. *Cell Death Dis.* **12**, 1102. doi:10.1038/s41419-021-04273-8
- Teixeira, L., Rabouille, C., Rørth, P., Ephrussi, A. and Vanzo, N. F. (2003). Drosophila Perilipin/ADRP homologue Lsd2 regulates lipid metabolism. *Mech. Dev.* **120**, 1071-1081. doi:10.1016/S0925-4773(03)00158-8
- Thibault, S. T., Singer, M. A., Miyazaki, W. Y., Milash, B., Dompe, N. A., Singh, C. M., Buchholz, R., Demsky, M., Fawcett, R., Francis-Lang, H. L. et al. (2004). A complementary transposon tool kit for Drosophila melanogaster using P and piggyBac. *Nat. Genet.* **36**, 283-287. doi:10.1038/ng1314
- Tootle, T. L. (2013). Genetic insights into the in vivo functions of prostaglandin signaling. *Int. J. Biochem. Cell Biol.* **45**, 1629-1632. doi:10.1016/j.biocel.2013.05.008
- Tootle, T. L. and Spradling, A. C. (2008). Drosophila Pxt: a cyclooxygenase-like facilitator of follicle maturation. *Development* **135**, 839-847. doi:10.1242/dev.017590
- Tran, S. L. and Welte, M. A. (2010). In-vivo centrifugation of Drosophila embryos. *J. Vis. Exp.* **40**, 2005. doi:10.3791/2005
- Walther, T. C. and Farese, R. V., Jr. (2012). Lipid droplets and cellular lipid metabolism. *Annu. Rev. Biochem.* **81**, 687-714. doi:10.1146/annurev-biochem-061009-102430
- Wang, H., Ma, W.-G., Tejada, L., Zhang, H., Morrow, J. D., Das, S. K. and Dey, S. K. (2004). Rescue of female infertility from the loss of cyclooxygenase-2 by compensatory up-regulation of cyclooxygenase-1 is a function of genetic makeup. *J. Biol. Chem.* **279**, 10649-10658. doi:10.1074/jbc.M312203200
- Wat, L. W., Chao, C., Bartlett, R., Buchanan, J. L., Millington, J. W., Chih, H. J., Chowdhury, Z. S., Biswas, P., Huang, V., Shin, L. J. et al. (2020). A role for triglyceride lipase brummer in the regulation of sex differences in Drosophila fat storage and breakdown. *PLoS Biol.* **18**, e3000595. doi:10.1371/journal.pbio.3000595
- Wattanakumtornkul, S., Damario, M. A., Stevens Hall, S. A., Thornhill, A. R. and Tummon, I. S. (2003). Body mass index and uterine receptivity in the oocyte donation model. *Fertil. Steril.* **80**, 336-340. doi:10.1016/S0015-0282(03)00595-8
- Weller, P. F. and Dvorak, A. M. (1994). Lipid bodies: intracellular sites for eicosanoid formation. *J. Allergy Clin. Immunol.* **94**, 1151-1156. doi:10.1016/0091-6749(94)90325-5
- Welte, M. A. (2015). As the fat flies: The dynamic lipid droplets of Drosophila embryos. *Biochim. Biophys. Acta* **1851**, 1156-1185. doi:10.1016/j.bbali.2015.04.002
- Welte, M. A., Cermelli, S., Griner, J., Viera, A., Guo, Y., Kim, D.-H., Gindhart, J. G. and Gross, S. P. (2005). Regulation of lipid-droplet transport by the perilipin homolog LSD2. *Curr. Biol.* **15**, 1266-1275. doi:10.1016/j.cub.2005.06.062
- Wheatley, S., Kulkarni, S. and Karess, R. (1995). Drosophila nonmuscle myosin II is required for rapid cytoplasmic transport during oogenesis and for axial nuclear migration in early embryos. *Development* **121**, 1937-1946. doi:10.1242/dev.121.6.1937
- White, R. P. and Welte, M. A. (2023). Visualizing lipid droplets in Drosophila oogenesis. *Methods Mol. Biol.* **2626**, 233-251. doi:10.1007/978-1-0716-2970-3_12
- Yen, C.-L. E., Stone, S. J., Koliwad, S., Harris, C. and Farese, R. V., Jr. (2008). Thematic review series: glycerolipids. DGAT enzymes and triacylglycerol biosynthesis. *J. Lipid Res.* **49**, 2283-2301. doi:10.1194/jlr.R800018-JLR200
- Yu, W., Bozza, P. T., Tzizik, D. M., Gray, J. P., Cassara, J., Dvorak, A. M. and Weller, P. F. (1998). Co-compartmentalization of MAP kinases and cytosolic phospholipase A2 at cytoplasmic arachidonate-rich lipid bodies. *Am. J. Pathol.* **152**, 759-769.
- Yue, F., Oprescu, S. N., Qiu, J., Gu, L., Zhang, L., Chen, J., Narayanan, N., Deng, M. and Kuang, S. (2022). Lipid droplet dynamics regulate adult muscle stem cell fate. *Cell Rep.* **38**, 110267. doi:10.1016/j.celrep.2021.110267
- Zhang, N., Wang, L., Luo, G., Tang, X., Ma, L., Zheng, Y., Liu, S., Price, C. A. and Jiang, Z. (2019). Arachidonic acid regulation of intracellular signaling pathways and target gene expression in bovine ovarian granulosa cells. *Animals (Base)* **9**, 374. doi:10.3390/ani9060374
- Zhao, X., Wang, W., Yao, Y., Li, X., Huang, X., Wang, Y., Ding, M. and Huang, X. (2022). An RDH-Plin2 axis modulates lipid droplet size by antagonizing Bmm lipase. *EMBO Rep.* **23**, e52669. doi:10.15252/embr.202152669

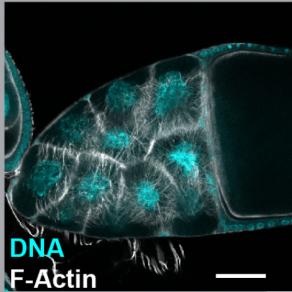
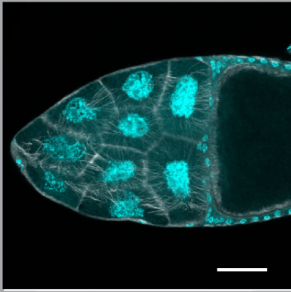
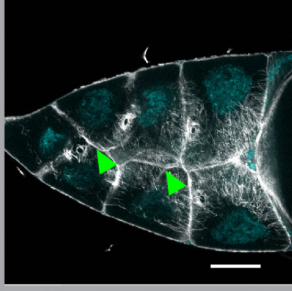
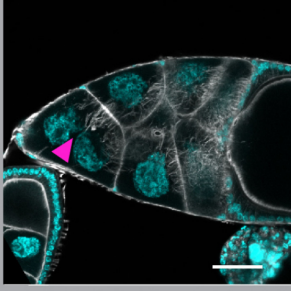
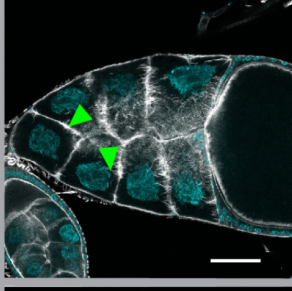
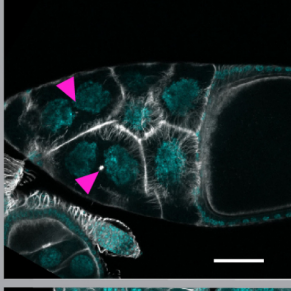
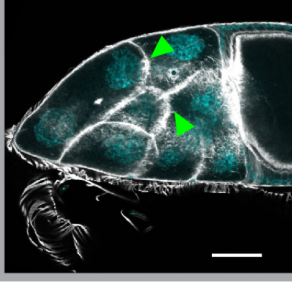
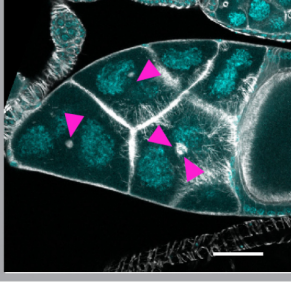
		Actin Bundles	Cortical Actin		
Normal		<p>Bundles form around nurse cell periphery</p> <p>Bundles are straight and oriented inward</p>		<p>Actin surrounds each nurse cell, separating nurse cell nuclei</p>	
	Mild		<p>Actin bundles are largely normal, but may be sparse, or missing from areas</p>		<p>Nurse cell nuclei are in close proximity/ touching</p> <p>A single instance of disrupted cortical actin is observed</p>
Defects	Moderate		<p>Actin bundles are sparse, stunted, and/or clumped</p> <p>Actin bundles are missing from areas around the nurse cell periphery</p>		<p>Two instances of disrupted cortical actin are observed</p> <p>Nurse cell nuclei are in close proximity/ touching</p>
	Severe		<p>Actin bundle formation is delayed, bundles fail to form, and are sparse and/or stunted and/or missing</p>		<p>Three or more instances of cortical actin breakdown are seen</p> <p>Nurse cell nuclei are in close proximity/ touching</p>

Fig. S1. Examples and criteria used for scoring actin remodeling phenotypes. Maximum projection of three confocal slices of representative S10B follicles stained for F-Actin (phalloidin) in white and DNA (DAPI) in cyan, and definitions of the indicated actin bundle and cortical actin phenotypes. Actin bundle and cortical actin phenotypes were independently binned into four categories: Normal, Mild Defects, Moderate Defects, or Severe Defects. Images were brightened by 30% to increase clarity. Arrowheads indicate examples of actin bundle defects (green), and cortical actin breakdown (magenta). Scale bars=50 μ m.

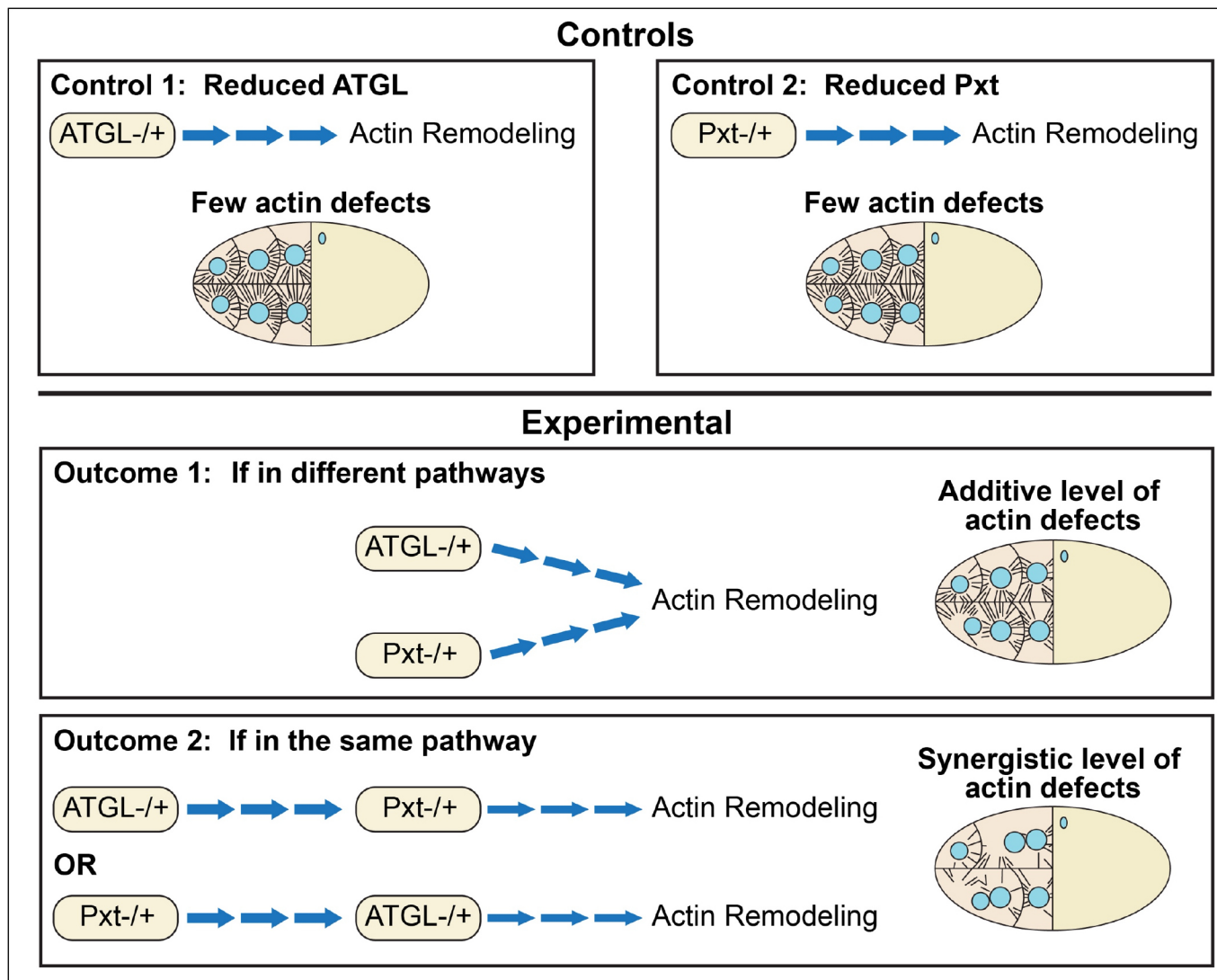


Fig. S2. Schematic of dominant genetic interactions.

Schematic of the premise of how dominant genetic interactions are used to determine if two factors act in the same pathway. Specifically shown are the controls and potential experimental outcomes for assessing if ATGL and Pxt function separately or together to control actin remodeling during S10B. The top depicts the Controls, single heterozygous follicles that have either reduced ATGL (**Control 1**) or reduced Pxt (**Control 2**); these control follicles are expected to have few actin defects. The bottom depicts the two possible experimental outcomes. **Outcome 1** depicts that ATGL and Pxt function in two separate pathways to regulate actin remodeling. In this case, the double heterozygous follicles will have actin defects that are similar to or additive of those seen in the control conditions. **Outcome 2** depicts that ATGL and Pxt function in the same pathway, with either ATGL acting upstream of Pxt or vice versa, to control actin remodeling. In this case, the double heterozygous follicles will exhibit a synergistic increase in actin defects that are more than additive of what is observed in the control conditions. The latter outcome is what is observed in Figure 4D-F.

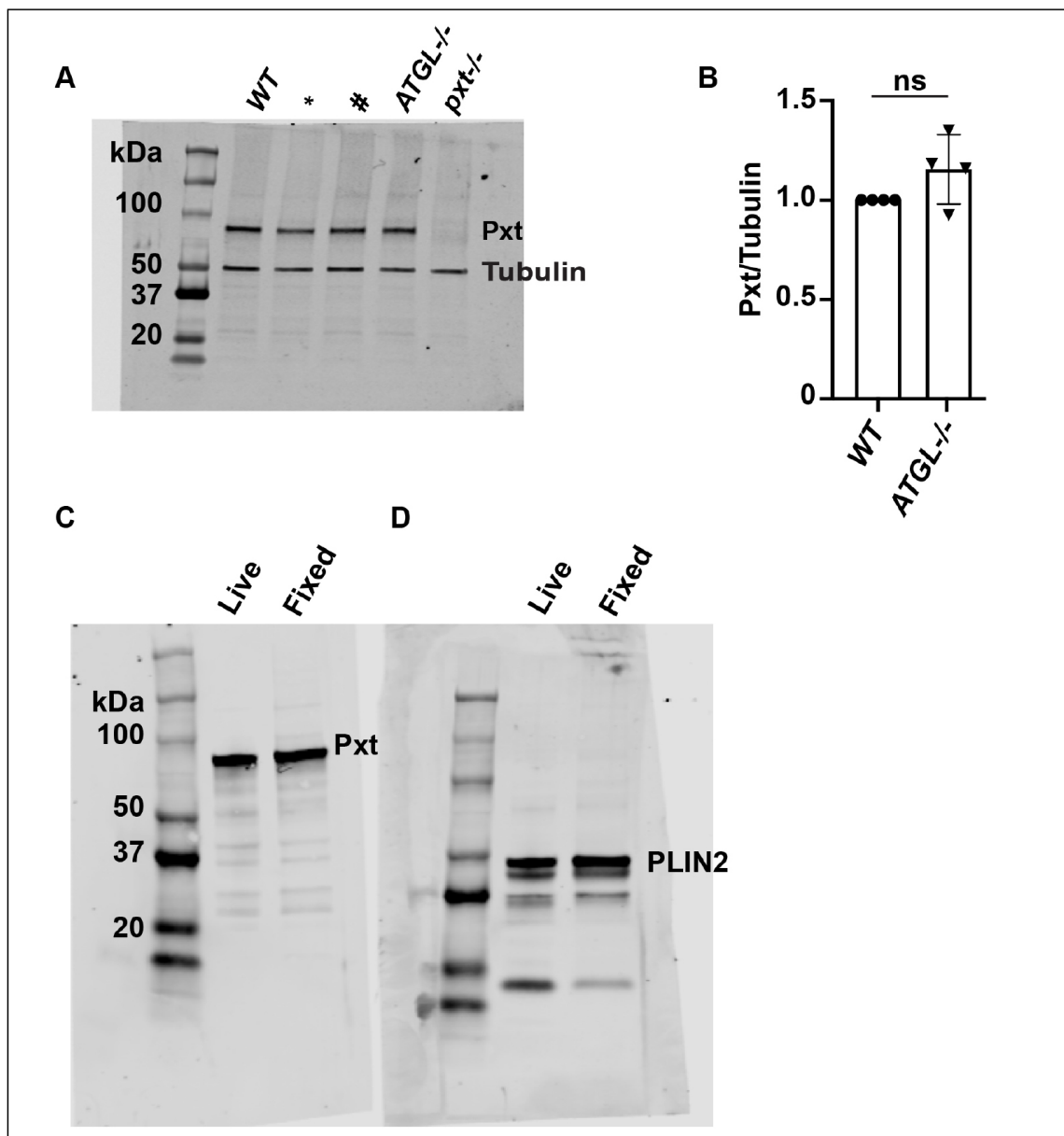


Fig. S3. ATGL does not affect Pxt expression.

(**A**) Immunoblot for Pxt and α -Tubulin of the indicated genotypes: WT, wild-type (Oregon R), *ATGL*^{-/-} (*bmm*¹/*bmm*¹) and *pxt*^{-/-} (*pxt*^{f01000}/*pxt*^{f01000}). The * and # lanes correspond to unrelated genotypes. (**B**) Quantification of **A**, in which band intensity was normalized as indicated. ns=p>0.05, unpaired t-test, two-tailed. (**C-D**) Immunoblots comparing the blotting patterns of live versus formaldehyde fixed wild-type whole ovary samples, 5 ovaries per lane, for Pxt (**C**) and PLIN2 (**D**). Loss of ATGL has no effect on Pxt levels (**A-B**). The live vs. fixed banding pattern is comparable for both Pxt (**C**) and PLIN2 (**D**) antibodies. Fixed samples were used in panel **A**.

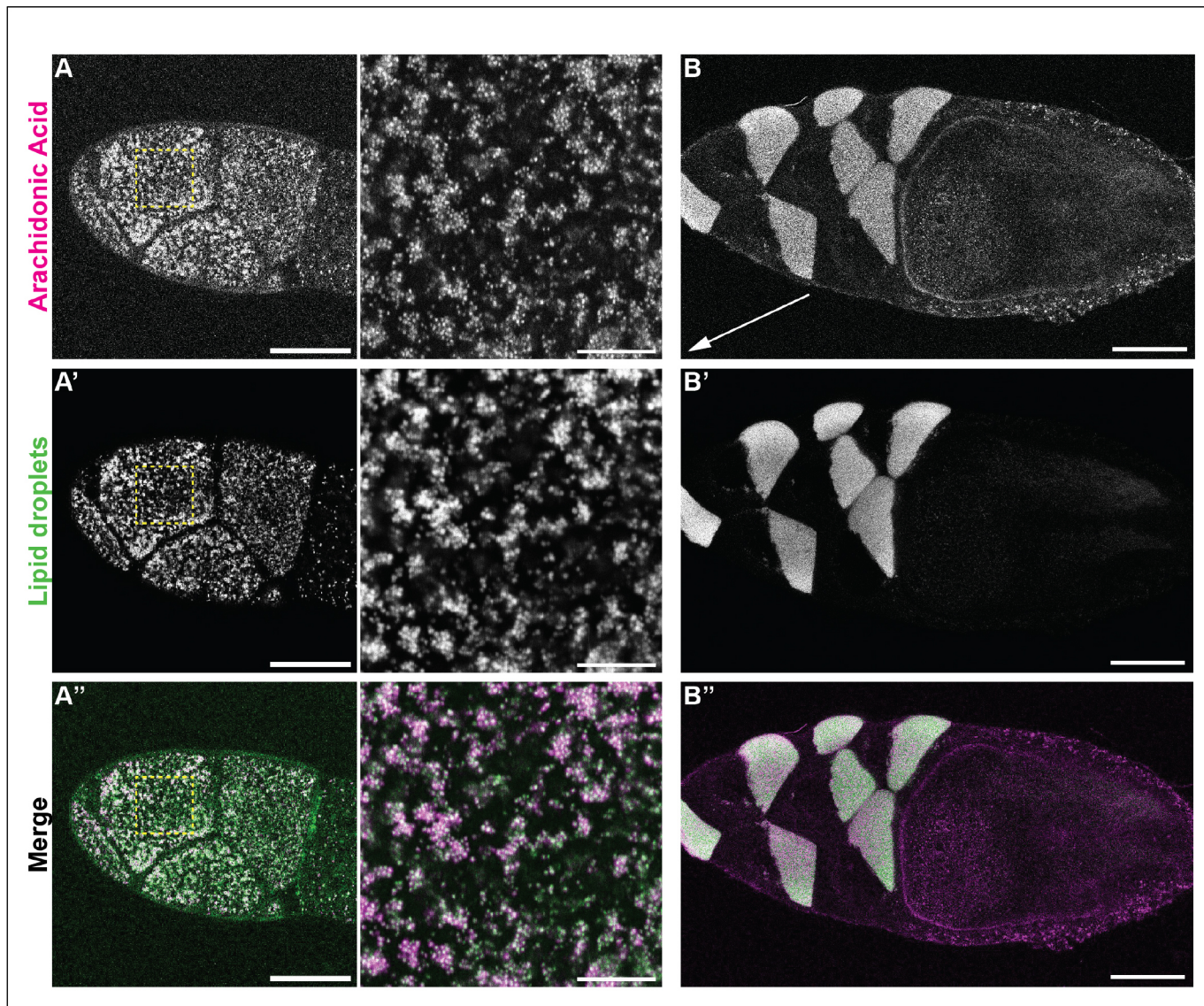


Fig. S4. AA from diet localizes to lipid droplets in Stage 10B follicles.

(**A-B''**) Confocal slice of live (**A-A''**, zoom-in of yellow boxed region) or (**B-B**) centrifuged wild-type (Oregon R) S10B follicles from flies fed 5 μ M NBD AA for ~12h, AA (green in merge) and LDs (LipidSpot, magenta in merge). In **A-A''** a focal plane near the nurse cell surface was chosen as LD density there is lower than in the center, making colocalization is easier to judge. In **B-B''** orientation of follicle during centrifugation is indicated by arrow. Scale bar = 50 μ m or 10 μ m (zoomed in images in A-A''). AA provided in the diet localizes to LDs in S10B follicles (**A-B''**).

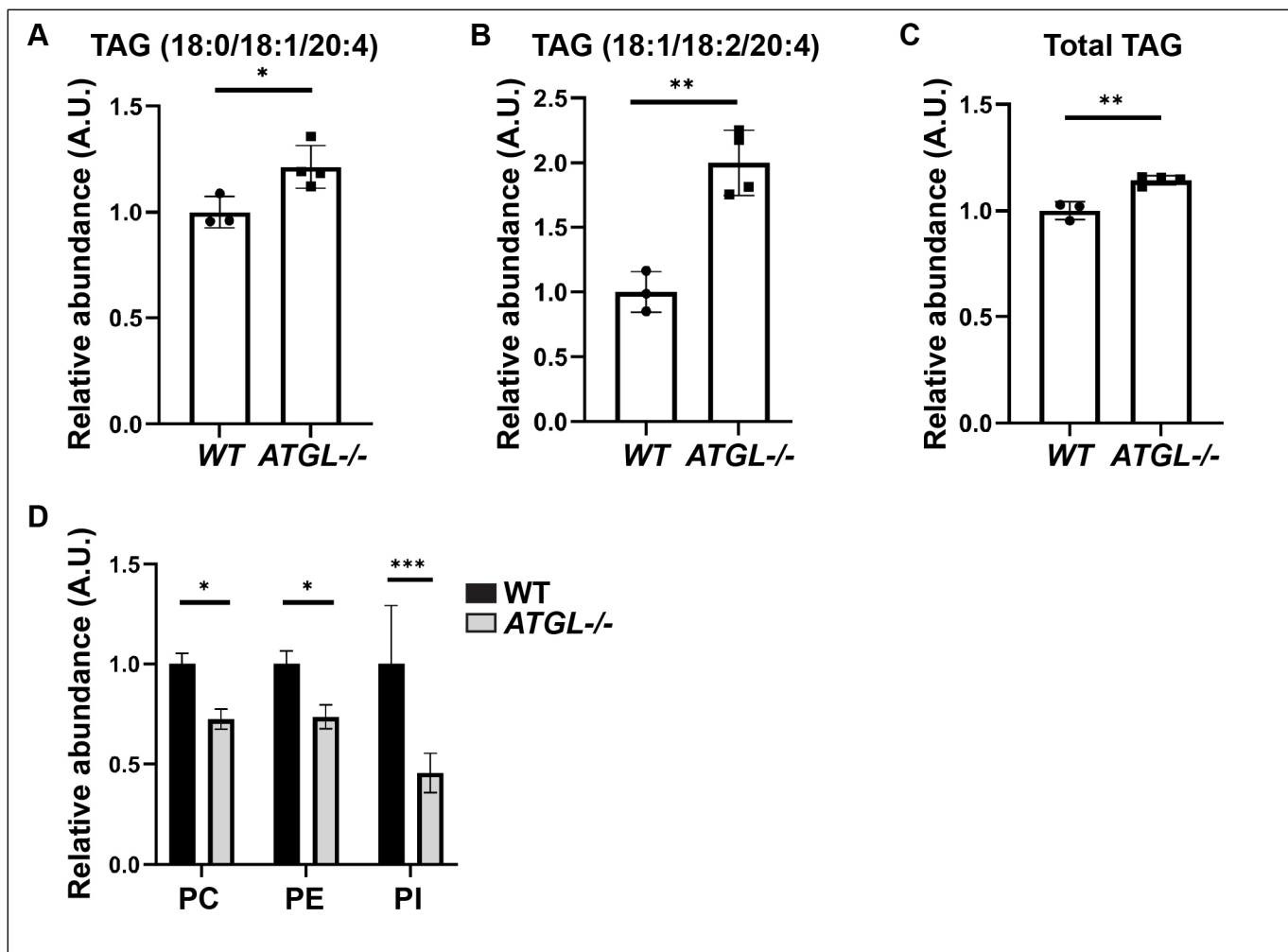


Fig. S5. AA-containing TAG and total TAG normalized to total lipids in sample.

(A-D) Lipids were extracted from wild-type (Oregon R) and *ATGL^{-/-}* (*bmm¹/bmm¹*) ovaries and analyzed by mass spectrometry. Data from Figure 6 re-plotted as relative abundance normalized to total lipids in the sample. Error bars, SD. (A, B) Two triglyceride species containing arachidonic acid (AA). Error bars, SD, * $p=0.0279$, ** $p=0.0019$, unpaired t-tests, two-tailed. (C) Overall triglyceride levels are slightly increased in *ATGL^{-/-}* ovary lipids. Error bars, SD, ** $p=0.002$, unpaired t-test, two-tailed. (D) Relative amounts of phosphatidylcholine (PC), phosphatidylethanolamine (PE), and phosphatidylinositol (PI) in wild-type versus *ATGL^{-/-}* ovary lipids. Error bars, SD, * $p=0.0329$, * $p=0.0416$, *** $p=0.0001$, Sidak's multiple comparisons test. While overall triglyceride levels are similar between the two genotypes (C), the AA-containing triglycerides are increased (A, B), and three classes of phospholipids are decreased (D) in the absence of ATGL. The reason for the decrease in phospholipids is not clear. One possibility is that ATGL breaks down triglycerides to generate precursors for phospholipid production; alternatively, in the absence of ATGL, ovaries may contain a different mix of follicle stages (and thus different levels of triglyceride accumulation) due to altered developmental progression.

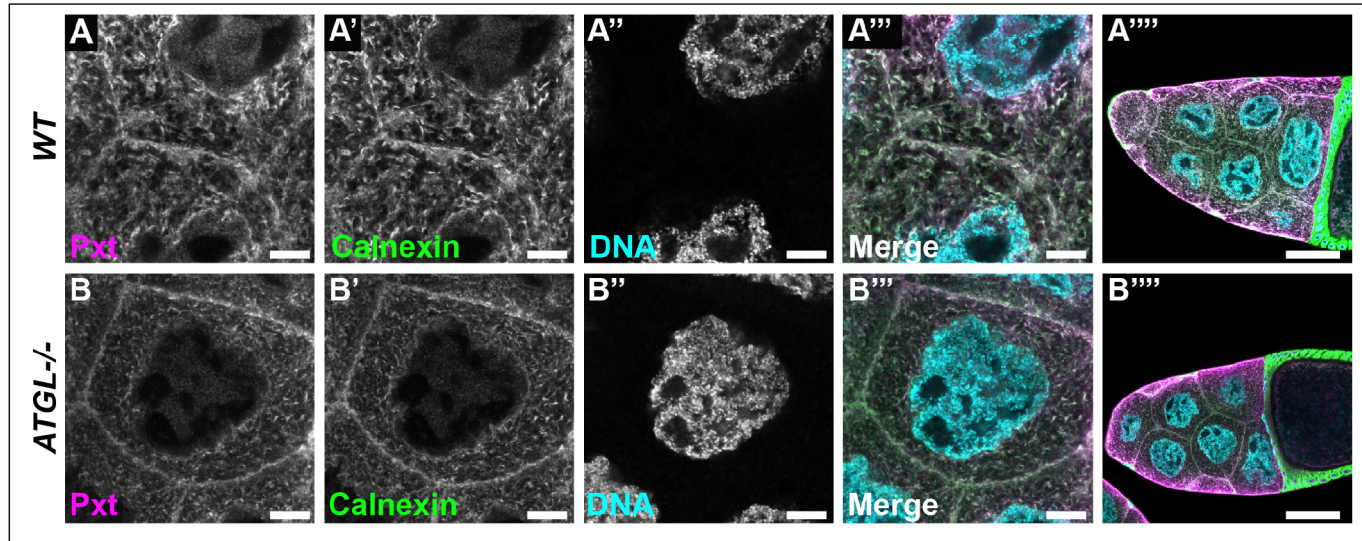


Fig. S6. ATGL does not affect Pxt's localization to the ER.

(A-B''') Single confocal slice of S10B nurse cells of the indicated genotypes, stained for Pxt (A-B), Calnexin (A', B', ER marker), and DNA (A'', B'', Hoechst). Merged images (A'''-A''', B'''-B'''): Pxt, magenta; Calnexin, green; and DNA, cyan. Genotypes: WT, wild-type (Oregon R); *ATGL*^{-/-} (*bmm*¹/*bmm*¹), and *pxt*^{-/-} (*pxt*^{f01000}/*pxt*^{f01000}). Scale bars = 10µm, except in A'''' and B'''' where = 50µm. Black boxes were added under panel and/or channel labels in A, A' and A''' to aid in visualization. In S10B follicles, Pxt's localization to the ER is similar to wild-type (A-A''') in *ATGL* mutants (B-B''').

Table S1. Quantitation of triglyceride species in ovaries

Column A lists the fatty acid content of various triglyceride species detected in ovaries by lipidomics. Columns B through H show the relative amount of those species in three wild-type (Oregon R) and four ATGL^{-/-} (*bmm¹/bmm¹*) samples. Reads are background corrected. A fourth wild-type sample was discarded as an outlier because the detected lipid amounts were an order of magnitude lower than in the other samples.

[Click here to download Table S1](#)

Table S2. Key Resources Table.

[Click here to download Table S2](#)

Table S3. Genotype by figures.

List of genotypes shown in the figures. * indicates phenotypic example of genotype not related to the data presented in the manuscript.

[Click here to download Table S3](#)

Table S4. Raw data.

Raw data used for all quantifications presented in both the primary and supplemental figures.

[Click here to download Table S4](#)